Cuticle chemistry drives the development of diffraction gratings on the surface of *Hibiscus trionum* petals

Edwige Moyroud[1,2,3,*], Chiara A. Airoldi[1], Jordan Ferria[1], Chiara Giorio[4], Sarah S. Steimer[4,5,6], Paula J. Rudall[7], Christina J. Prychid[7], Shannon Halliwell[1], Joseph F. Walker[2], Sarah Robinson[1,2], Markus Kalberer[4,5], and Beverley J. Glover[1,*]

Affiliations

[1] Department of Plant Sciences, University of Cambridge, Downing Street, Cambridge CB2 3EA, UK

[2] The Sainsbury Laboratory, University of Cambridge, 47 Bateman Street, Cambridge CB2 1LR, UK

[3] Department of Genetics, University of Cambridge, Downing Street, Cambridge CB2 3EH, UK

[4] Yusuf Hamied Department of Chemistry, University of Cambridge, Lensfield Road, Cambridge CB2 1EW, UK

[5] Department of Environmental Sciences, University of Basel, Klingelbergstrasse 27, 4056 Basel, Switzerland

[6] Department of Environmental Science, Stockholm University, 106 91 Stockholm, Sweden

[7] Royal Botanic Gardens Kew, Richmond, Surrey TW9 3AB, UK

* Corresponding Authors: Edwige Moyroud (em500@cam.ac.uk) and Beverley J. Glover (bjg26@cam.ac.uk)

Lead Contact: Edwige Moyroud

Twitter Handles:
@Edwige_M
@Beverley_CUBG

Summary

Plants combine both chemical and structural means to appear colourful. We now have an extensive understanding of the metabolic pathways used by flowering plants to synthesize pigments, but the mechanisms remain obscure whereby cells produce microscopic structures sufficiently regular to interfere with light and create an optical effect. Here, we combine transgenic approaches in a novel model system, *Hibiscus trionum*, with chemical analyses of the cuticle, both in transgenic lines and in different species of *Hibiscus,* to investigate the formation of a semi-ordered diffraction grating on the petal surface. We show that regulating both cuticle production and epidermal cell growth is insufficient to determine the type of cuticular pattern produced. Instead, the chemical composition of the cuticle plays a crucial role in restricting the formation of diffraction gratings to the pigmented region of the petal. This suggests that buckling driven by spatio-temporal regulation of cuticle chemistry could pattern the petal surface at the nanoscale.

Keywords

Cuticle patterning, Diffraction gratings, *Hibiscus*, Mechanical buckling, Petal development, Plant epidermis, Structural colour

Introduction

Colour is a conspicuous feature of many living organisms, playing important roles in signalling to repel predators and rivals, lure prey, or attract mates. Organisms can produce pigments that absorb subsets of light to generate colour or instead produce nanoscale structures made of transparent material to reflect particular wavelengths of light [1–3]. These structural colours often produce different hues according to the angle from which the subject is viewed - the phenomenon of iridescence. The minute structures responsible for such coloured optical effects are found in both animals and plants. Their morphologies are well characterized and the physical mechanisms underpinning colour production in each case have been identified through optical measurements and theoretical simulations [4–6]. However, the biological processes controlling the construction of such optical devices during development remain largely unexplored. In plants, structural colours are commonly

produced by multi-layer reflectors or by pseudo-regular parallel surface striations acting as diffraction gratings[5,7–9]. Diffraction gratings consist of an ordered system of ridges and grooves with a specific periodicity that diffracts light and allows constructive interference for different reflected wavelengths at different angles. How plants develop such structures on their surface remains to be understood.

Here we use diffraction gratings on petals as an experimental system to address this question. Examples of diffraction gratings have been found in flowers across all angiosperm lineages except the earliest-divergent lineages, and this optical element is likely to have evolved independently multiple times in the flowering plants [10,11]. Petal diffraction gratings are made of semi-ordered striations of the cuticle, a waxy polymer that covers the surface of all plant aerial organs [11,12]. The presence of disorder in the grating creates weak iridescence and a blue halo - scattered light in the blue-UV part of the spectrum - that is perceived by bumblebees and can enhance their foraging efficiency in laboratory conditions [11].

As conventional models do not produce structurally coloured flowers, we developed *Hibiscus trionum* (Malvaceae) as an experimental system to explore diffraction grating development. This species has a short life cycle (seed to flowering in ~7 weeks); it is easy to grow in a range of conditions, readily self-fertilises and can also be cross-pollinated. The adaxial petal surface is demarcated into two regions, a white distal region with smooth conical and isodiametric epidermal cells and a heavily pigmented purple proximal region where the epidermal cells are flat, elongated (tabular) and topped with parallel cuticular ridges that are partially disordered and create the blue sheen visible at the petal base [10–12].

Previous studies have postulated that the striations on the petal surface of *H. trionum* and other species form through mechanical buckling [13–15]. Several related but distinct models speculate that the striations develop due to the presence of compressive stresses in the cuticle during petal development. The stress is hypothesised to be generated by conflicting pressures arising from anisotropic growth of the epidermal cells and their walls and simultaneous isotropic production of cuticle by those same cells. The mechanical stress on the cuticle would generate the instability that causes the cuticle to buckle, producing a system of semi-ordered ridges

[13–15]. Recent work in support of a mechanical model for diffraction grating development showed that applying mechanical stress to isolated *H. trionum* petal tissue can induce the formation of striations in the cuticle of the pigmented region [15].

The simplest and earliest of the models to explain petal diffraction grating formation through mechanical buckling was proposed by Antoniou-Kourounioti and colleagues [13]. This model suggested that petal surface patterning could be predicted from only two sets of parameters - the anisotropic growth of the cell and the rate of cuticle production (specifically, whether cuticle production kept pace with, exceeded, or fell behind cell growth). More recent models proposed an alternative scenario in which the cuticle consists of a bilayer system, with the relative stiffness of the two layers playing a key role alongside their thickness and the growth of the cell [15].

Here we test the simple model of Antoniou-Kourounioti and colleagues [13], and examine whether cuticle production and anisotropic cell growth are sufficient parameters to explain the cuticular patterns found on petal surfaces. We take advantage of the natural diversity of petal surfaces found in different species of *Hibiscus*; we also developed a protocol to transform *H. trionum* and manipulate gene expression *in planta*. Our results indicate that regulating cell growth and the rate of cuticle production is not sufficient to control cuticular patterning. Instead, our results implicate the chemical composition of the cuticle as an essential factor to diffraction grating formation. We propose that the *Hibiscus* petal cuticle could function as a self-organising material, with chemistry-driven buckling patterning the petal surface at the nanoscale.

Results and discussion

Striation formation coincides with anisotropic cell growth

To start investigating striation formation, we characterized in detail the cell differentiation process on the adaxial epidermis of *Hibiscus trionum* petals throughout bud development (Figure 1A). At stage S1, petal primordia are green, and the epidermal cells appear isotropic and undifferentiated across the entire petal surface (Figures 1B-1D): their cuticle is smooth and anthocyanin pigments are absent, only starting to appear at the very base of the petal in late S1 (Figure 1B). Two distinct regions emerge

on the petal surface at S2 as only cells in the proximal region of the petal epidermis accumulate anthocyanin. Cuticular striations are initiated between S3 and S4 and are also restricted to the proximal pigmented region. The unpigmented cells in the distal portion of the petal remain smooth (Figures 1C and 1D). Striation formation is concurrent with anisotropic cell expansion as epidermal cells in the proximal region start to elongate along the base-to-tip petal axis from S3 onwards (Figure 1D). Cells in the distal region instead mostly expand perpendicularly to the petal surface, acquiring their characteristic conical shape. Thus, cuticular striations emerge simultaneously with anisotropic cell growth.

Measurement of cuticle thickness and cell expansion is insufficient to predict cuticular patterns

The early model proposed by Antoniou-Kourounioti and colleagues [13] describes how different degrees of anisotropic cell elongation and cuticle production result in mechanical stress. Specifically, the model proposes that where the amount of cuticle produced keeps pace with cell growth and cuticle thickness remains constant, the cuticle layer will be stress-free, but when cuticle production rate is inconsistent with cell growth, then compressive or tensile stresses will occur. To release this stress, the cuticle buckles and forms striations [13]. To test whether a change in cell expansion (in magnitude and direction) would lead to a change in cuticular pattern, as predicted by the model, we first applied chemical treatments to developing *H. trionum* buds before striation formation (<S3) and recorded the cuticular patterns observed once flowers open (S5). Ectopic application of cytoskeletal drugs or plant hormones successfully modified cell expansion in the proximal region of the petal epidermis, but striations were always produced, regardless of changes in cell dimension (Figure S1).

This result is consistent with the predictions of the theoretical model (Figure 2A) and confirms experimentally that cuticular pattern topology is resistant to cell growth variations when those fall within the range defined by the model. As chemical treatments did not allow us to cross model boundaries, we used natural diversity to enhance our exploration of the possibility space and access other cell behaviours (Figures 2B and 2C). We selected different accessions and species from the Trionum and Phylloglandula sections of *Hibiscus* (Data S1) and compared the cuticular pattern observed in the proximal region of the adaxial petal epidermis with the pattern predicted by the model. According to the model, the parameter values measured in all cases (cell

expansion and cuticle production, Table S1) should induce striation formation (Figures 2D-2F). However, the petal epidermal cells of *H. sabdariffa*, *H. cannabinus* and *H. trionum* (Botswana accession) are all completely smooth (Figure 2B). Therefore, we conclude that the cell growth and change in cuticle thickness recorded in related *Hibiscus* species do not always generate the predicted pattern (Figures 2D and 2E). This result indicates that the model of Antoniou-Kourounioti and colleagues[13] is not sufficient to predict petal cuticle patterning in *Hibiscus*.

Interfering with cuticle production is sufficient to modify cuticular patterning

To determine whether varying cuticle production could affect diffraction grating assembly, we used a transgenic approach to misexpress genes encoding enzymes or transcriptional regulators contributing to the synthesis or assembly of cuticular components in other species. First, we interfered with cuticle structure by constitutively expressing *CUTICLE DESTRUCTING FACTOR1* from Arabidopsis, *AtCDEF1* (Figure S2A). *AtCDEF1* encodes a GDSL lipase-esterase that disrupts cuticle integrity when overexpressed in Arabidopsis[16]. Flowers from *Hibiscus trionum 35S:AtCDEF1* appear similar to wild type in terms of petal size/shape, pigmentation pattern and cell shape, but lack the bluish tinge in the proximal region of the petal (Figures 3A, 3D and 3G). Closer examination revealed that the striated portion of the petal was greatly reduced and discontinuous, with cuticular ridges found only on irregular patches of cells towards the petal base (Figures 3B, 3C, 3E, and 3F versus Figures 3H and 3I). Thus, impairing ordinary cuticle assembly is sufficient to disrupt diffraction grating formation in *H. trionum*. Reciprocally, we also aimed to evaluate the effects of cuticle overproduction on epidermal texture. In *Arabidopsis thaliana*, the SHINE1 transcription factor from the AP2/EREBP-like superfamily plays a key role in driving cuticle production[17–19].

The *SHINE A* lineage to which Arabidopsis *SHINE1* belongs appears to be lost in Malvaceae, as we found no orthologs in the genomes of cotton (*Gossypium raimondii*) or cocoa (*Theobroma cacao*) (Figure 3J; Data S2). However, we identified three *SHINE-like* genes in *H. trionum*. Our phylogenetic analysis (Figure 3J) shows that *HtSHINE1* belongs to the *SHINE B* clade, which also contains the other two Arabidopsis homologs, *SHINE2* and *SHINE3*. The remaining two *Hibiscus SHINE* genes belong to the *SHINE C* lineage, which has no Arabidopsis representative (Figure 3J). To identify which *Hibiscus SHINE*, if any, was most likely to control cuticle

production where the diffraction grating forms, we used quantitative RT-PCR to follow
172 their expression throughout petal development (Figure 3K). We found that *HtSHINE1* (*HtSHN1*) and *HtSHINE2* (*HtSHN2*) are both expressed at very low levels across the
174 petal and by S3 corresponding transcripts are barely detectable in the proximal region, where striations are about to initiate. In contrast, *HtSHINE3* (*HtSHN3*) transcription is
176 restricted to the proximal region and increases dramatically from S2 to S4, reaching expression levels two hundred times higher than the maximum levels recorded during
178 petal development for the other two *HtSHINE* homologs (Figure 3K). The spatio-temporal expression pattern of *HtSHN3* makes it a strong candidate for regulating
180 cuticle production at the petal base as diffraction gratings emerge. To test whether HtSHN3 was able to induce striation formation, we expressed *HtSHN3* constitutively
182 in *H. trionum* using the Arabidopsis *UBQ10* promoter (Figure S2B). During the vegetative phase, *UBQ10:HtSHN3* plants showed characteristic signs of cuticle defects
184 including slower growth and smaller leaves with curled margins (Figure S3A), also observed in Arabidopsis when *SHINE1* is overexpressed[18]. Once plants started to
186 flower, constitutive expression of *HtSHN3* was sufficient to trigger striation formation in the cuticle of some epidermal cells that are ordinarily smooth in wild type. On the
188 adaxial petal epidermis of *UBQ10:HtSHN3* flowers, the tabular smooth cells located in the transition zone between the purple and the white part of the petal occasionally
190 developed a striated cuticle (Figure 3L, compared with Figure S3B). Ectopic striations were also recorded on the usually smooth abaxial petal surface (Figures S3C and S3D),
192 covering individual patches of tabular and puzzle cells in the proximal and distal regions, respectively (Figures 3M and 3N). Taken together, these results indicate that
194 constitutive expression of *HtSHN3* can induce ridge emergence on otherwise smooth cells, but the effects are uneven: only small groups of isolated cells gain striations while
196 the surface of most cells remains unchanged (Figure 3L-3N).

To modify cell surface patterning more extensively across the petal, we fused
198 the strong viral activation domain VP16 [20] or the transcriptional silencing motif SRDX (EAR repressor motif of Arabidopsis *SUPERMAN* [21]) to HtSHN3. Surprisingly, when
200 overexpressed in *Hibiscus* (Figures S2E and S2F) both fusion proteins generated identical phenotypes, characterised by complete lack of striation in the proximal region
202 of the petal (Figures 4A-4F). This is not due to compensatory ectopic expression of *HtSHN1* or *HtSHN2* in the proximal region of the petal, as quantitative RT-PCR
204 confirmed that both genes remain expressed at very low levels (Figures S2H and S2I).

To gain insight into the underpinning mechanisms accounting for these phenotypes, we examined the expression of potential target genes of HtSHN3 in both types of transgenic lines. Transcriptomic analyses in Arabidopsis identified genes whose expression is affected when *SHN1* or *SHN1-SRDX* is overexpressed [22]. These genes include members of the Cytochrome P450 family 77 (i.e., *At3g10570*) and genes coding for GDSL-motif lipases/hydrolases (i.e., *At2g04570*). We isolated *Hibiscus trionum* sequences homologous to *At3g10570* (*HtCYP77*) and *At2g04570* (*HtGDSL*) and compared their expression levels in wild type and lines overexpressing *HtSHN3-SRDX* or *HtSHN3-VP16* (Figure 4G). Both *HtCYP77* and *HtGDSL* are downregulated in *35S:HtSHN3-SRDX*, consistent with results obtained in Arabidopsis. Contrary to our initial assumption, *HtCYP77* and *HtGDSL* are also downregulated in plants overexpressing *HtSHN3-VP16* (Figure 4G). This could explain why both types of transgenic lines exhibit the same lack-of-striation phenotype. We hypothesize that the addition of the VP16 domain may have impaired the ability of HtSHN3 to activate transcription by influencing its folding or its ability to interact with DNA or other proteins. Taken together, our data indicate that interfering with cuticle production in *Hibiscus* is sufficient to modify surface texture in petal epidermis.

The chemistry of the petal cuticle is a key factor controlling pattern formation

The cuticular pattern variations we observed after manipulating *HtSHN3* expression and/or activity could be due to quantitative (cuticle thickness) or qualitative (cuticle components) changes. Indeed, previous studies in Arabidopsis and Tomato have shown that both the amount and composition (components of and relative amounts of cutin, waxes and other secondary metabolites) of the cuticular layer are altered when *SHN-like* genes expression levels are modified [18,23].

To examine whether striation absence coincides with a reduction in cuticle synthesis during *Hibiscus* petal development, we used a Fat Red assay to stain the cuticle of petal cross-sections in the proximal region of wild type and *35S:HtSHN3-VP16* lines. This revealed no significant difference in cuticle thickness at stage 5 (Figures 4H and 4I), suggesting that other regulators of cuticle synthesis have a greater influence on cuticle production rate. Similarly, CryoSEM fractures of the petal adaxial epidermis proximal region did not uncover any difference in architecture of the cuticle and cell wall between wild type and *HtSHN3-VP16* or *HtSHN3-SRDX* lines (Figure S4). Next, we estimated cuticle production rate β (STAR Methods; Figures

S1H-S1J), which measures whether cuticle growth keeps pace with cell growth. There were differences in cuticle thickness at S3, which resulted in some variation in the cuticle production rate β between lines and therefore the predicted stresses. We also estimated the expansion experienced by cells in the proximal region of the petal adaxial epidermis in the various *HtSHN3* transgenic lines (Figures 4J and 4K) and used our theoretical model to infer the expected surface pattern. According to the model, proximal tabular cells from these transgenic lines should all develop cuticular striations, despite small changes in the β and expansion parameters (Figures 4J and 4K), but they do not. Such discrepancies between predicted and observed patterns are reminiscent of our earlier observations for other *Hibiscus* species (Figures 2B, 2D, and 2E). Developmental models try to simplify processes occurring in living tissues. When they are proven incorrect by experimental data this often indicates that parameters are missing and/or that the model is too simple. For instance, the theoretical model we used does not take into account the nature of the cuticular material. As *SHINE* homologs could also influence cuticle composition, we hypothesised that the absence of striations even when the conditions should induce buckling according to the model, could be due to a change in cuticle chemical components. This would modify the mechanical properties or structure of the cuticle, altering the system behaviour under compressive stresses and its propensity to buckle.

To test this hypothesis, we used a transgenic approach to alter cuticle chemistry. MYB106 and MYB16, members of the MIXTA-like class of MYB transcription factors [24], act redundantly in Arabidopsis to induce wax biosynthesis [22]. Waxes are important components of the cuticle and are likely to reduce water permeability on the plant surface. We isolated a *MIXTA-like* gene, *HtMIXTA-like1,* from *H. trionum* petals and used the strong CaMV 35S promoter to drive its expression constitutively *in planta* (Figure S2C). The metallic blue sheen characteristic of the petal proximal region appeared greatly reduced in *35S:HtMIXTA-like1* (*35S:HtML1*) flowers (Figure 4L). This also coincides with the disappearance of striations: the cuticle overlaying the pigmented epidermal cells in *35S:HtML1* plants appears mostly smooth with only patches of striated cells remaining (Figures 4M-4P). When present, striations are shallow and less prominent than in wild type (Figures 4O and 4P).

Studies in Arabidopsis have also identified a second regulator of wax production, Decrease Wax Biosynthesis (DEWAX), an AP2/ERF factor that

transcriptionally represses wax biosynthetic genes [25]. To alter wax production, we introduced a *35S:AtDEWAX* construct into *Hibiscus trionum* (Figure S2G). The resulting plant showed no obvious phenotypic defect except for disruption of diffraction grating formation (Figures 5A-5C). In wild type, cuticular striations are continuous between epidermal cells so that individual cells are hard to distinguish (Figure 5D, see also Figure 1D Stage 5 or Figure 3I). However, in the *35S:AtDEWAX* line, cell outlines are extremely prominent with the cuticle accumulating over the cell-cell junctions (Figures 5A and 5B). Striations within a cell area were sometimes completely missing, but most often misaligned (Figure 5B) or severely disrupted (Figure 5C). The observation that altering wax content disrupts striation development has not been made in Arabidopsis, possibly as a result of the different chemistries and material properties of different cuticles.

Cutin is a polyester of hydroxy fatty acids that forms a matrix in which compounds including waxes and phenolics are embedded [26]. The *CUTIN DEFICIENT1* (*CD1*) gene from Tomato and its homologs in Arabidopsis belong to a family conserved across land plants coding for cutin synthase-like (CUS) proteins that catalyse the formation of cutin oligomers [27–29]. In Arabidopsis CUS2 is necessary for the maintenance of the irregular cuticular ridges that usually cover sepals [30]. We isolated a CUS family member from our *H. trionum* petal cDNA library, *HtCUS1*, and produced a series of transgenic lines overexpressing *HtCUS1* (Figure S2D). These plants showed phenotypes typically associated with cuticular defects, such as fusion between neighbouring organs (Figure S5A). They also showed loss of conspicuous blue sheen at the flower centre (Figures S5D and S5E). Closer inspection of the petal surface confirmed that diffraction grating formation is impaired: when present, cuticular striations are faint and interrupted, and often short and restricted to the junction between neighbouring cells (Figures 5E and 5F compared with Figures 5G and S5F-S5N). This reduction in cuticular striation is not petal-specific as the disordered striations that cover the adaxial side of wild type *H. trionum* leaves (Figure S5B) are mostly absent in *35S:HtCUS1* plants (Figure S5C).

Our results point toward a key role for cuticle composition and/or arrangement of its constituents in diffraction grating formation. *CUS* gene silencing in tomato led to a decrease in cutin density caused by a reduction in ester bond formation and the presence of nanopores in the polymer [27]. Therefore, *CUS* overexpression may change the degree of cutin reticulation: additional cutin synthase activity could lead to the

production of a more densely cross-linked polymer and, thus, a cuticle with distinct mechanical properties, in particular a different degree of stiffness. The stiffness of a film is a significant determinant of its ability to buckle [31–33]. Transgenic lines and natural species devoid of striations (Figures 2B, 4C, and 4E) could share similar cuticle composition and thus mechanical properties.

To examine in more detail the relationship between cuticle composition and diffraction grating formation in *Hibiscus trionum*, we analysed the chemical composition of the cuticle from different transgenic lines using a LESA-MS method (liquid extraction surface analysis coupled with a high-resolution mass spectrometer), which we previously developed and validated using wild type *H. trionum* petals [34]. In LESA-MS the surface of a sample is probed selectively, while deeper layers of the sample are not extracted and analysed. We conducted a Principal Component Analysis (PCA) on the compounds detected in the cuticle of the various transgenic lines, which revealed that Principal Component 1 (PC1) can resolve samples with a striated cuticle from smooth ones (Figure 6A). This result confirms the link between cuticle chemistry and patterning and suggests that cuticle composition is a useful parameter to consider when attempting to predict the texture that differentiating epidermal cells will display on their surface. Closer examination of the LESA-MS data singled out candidate components most likely to account for this partitioning: the presence of free (unpolymerized) 10,16-dihydroxyhexadecanoic acid, a key monomer of cutin also known as dihydroxy-palmitic acid, and very long chain fatty acids (waxes) appear to strongly associate with striated samples, while potentially phenolic compounds such as $C_{27}H_{28}O_{19}$, $C_{27}H_{28}O_{18}$, $C_{26}H_{26}O_{17}$ and $C_{26}H_{26}O_{18}$ tend to be detected in smooth cuticles (Table S2). Using FTIR spectroscopy, Mazurek and colleagues showed that remaining cutin monomers are connected in a novel fashion when dihydroxy-palmitic acid is absent and several Arabidopsis mutants that only produce very low amounts of this specific cutin monomer also fail to form the usual stellate cuticular ridges on their petal conical cells [35–37]. These previous studies in Arabidopsis could not address the generation of structural colour, but they reinforce our conclusion that the presence of dihydroxy-palmitic acid may be essential for cuticle buckling and diffraction grating formation. Waxes and phenolic compounds can also impact the cuticle properties [38,39]. It has previously been reported in persimmon fruit that waxes impregnating the cutin network play a central role in toughening the cuticular layer [40]. Phenolic compounds such as flavonoids accumulate in the cuticle of multiple species. For instance, flavonoid

levels during cuticle biosynthesis have been shown to correlate with the number of ester bonds that form in the cutin polymer [41]. Once embedded in the cuticular layer, flavonoids could also act as stiffening nanofillers, altering cuticle mechanical properties and its propensity to deform [42]. Other compounds, such as $C_{32}H_{56}O_4$, also appear to make significant contributions to PC1 (Table S2A). However, while $C_{32}H_{56}O_4$ is almost always detected in samples with a striated cuticle, it is also present in almost half of the samples with a smooth surface (Table S2A). Thus, $C_{32}H_{56}O_4$ seems a less powerful predictor of the presence/absence of striation.

Next, we set out to characterise the chemical composition of a second independent set of cuticles by LESA-MS analyses on the petal surfaces of the different species of *Hibiscus* examined in Figures 2B and 2C. We expanded this sample set by characterising two *H. trionum* samples without a diffraction grating: (i) the abaxial (underneath) petal epidermis from mature *H. trionum* flowers and (ii) the adaxial surface of stage 3 petals that are yet to form cuticular striations (Figure 1D, stage 3). Here too, PCA identified a first PC that separates striated from smooth cuticular samples (Figure 6B). Similar to the observed result when using transgenic lines as samples (Table S2A), wax accumulation appears to characterise the striated cuticles while potentially phenolic compounds associate with smooth surfaces (Table S2B, Figures 6C and 6D). We also noted that half of the top 20 compounds are shared by both datasets (Table S2) when the compounds detected were ranked in each set according to their respective contribution to PC1 (Figures 6A and 6B). Probable phenolic compounds $C_{27}H_{28}O_{19}$ and $C_{27}H_{28}O_{18}$, the cutin monomer dihydroxy-palmitic acid and six potential waxes all show association with one type of cuticular pattern (smooth or striated). Thus, modifying cuticle chemistry, and possibly the chemistry of the entire cell wall-cuticle continuum, could be one of the mechanisms at work to modify cuticle patterning during both plant evolution and petal development. Indeed, changes targeting the biosynthetic pathways that produce these compounds could arise during evolution, triggering loss or gain of diffraction gratings in different *Hibiscus* lineages and accounting for the lability of iridescence across the genus. Regulatory changes affecting the same pathways could also occur during development from stage S3 onwards, to produce a cuticular material whose mechanical properties are suitable for diffraction grating formation on the surface of a growing petal. Previous work showed that striation formation via buckling can be induced by applying a mechanical force to the smooth proximal region (Figure 1D) of S3 *H. trionum* petal primordia (pre-

striation stage)[15]. To test whether differences in chemical constituents between striated and smooth cuticle correlate with differences in mechanical properties, we used a similar procedure to that described in [15] to apply in-plane mechanical stress to the proximal region of S3 pre-striation stage petals from transgenic *Hibiscus* lines with a smooth surface (*35S:HtSHN3-VP16* and *35S:HtSHN3-SRDX*) and wild type for comparison (Figure S6). Our results show that, while prominent cuticular ridges readily appeared on the surface of all pre-striation stages in wild type samples upon application of mechanical perturbation (Figure S6A), cuticular striations failed to form on the surface of both *35S:HtSHN3-VP16* and *35S:HtSHN3-SRDX* S3 petal primordia when an equivalent force was applied (Figures S6B and S6C). In wild type plants, striations are clearly visible on Stage S4 petal primordia (Figure 1D) but absent from *35S:HtSHN3-SRDX* and *35S:HtSHN3-VP16* as the transgenic lines produce petals with an entirely smooth adaxial surface (Figures 4A-4F and S6D). The application of an external force to S4 petal primordia from plants overexpressing *HtSHN3-VP16* was not sufficient to restore a wild type phenotype as most stretched cells remained smooth, with some cells occasionally exhibiting very short and faint striations (Figure S6D). Taken together, our results indicate that equivalent petal tissues regions, with similar cell geometry, dimensions, cuticle thickness, and architecture (Figures 4C-4F, 4H, 4I, and S4) but different cuticle chemical profiles, can vary in their buckling ability and thus their capacity to form a diffraction grating during development or upon application of a mechanical force.

LESA-MS data from this study (Figure 6) and from Giorio *et al.* (2015) [34] demonstrate distinct chemical profiles between the striated and non-striated portions of the same petal, we have also shown the spatially restricted expression of a key transcription factor, *HtSHINE3*, involved in the production of cuticle components in the proximal region of the petal (Figure 3K). Previous studies have reported distinct cuticular properties of different epidermal cell types [43], but our work indicates that cuticle chemistry can be controlled with exquisite spatial resolution across fields of cells within a single organ, allowing different regions of the same epidermis to exhibit different mechanical behaviours and surface textures that themselves cross boundaries of multiple cells.

Conclusion

Here we demonstrate experimentally that cell surface patterning in petals is resistant to cell growth variations that fall within the range predicted by theoretical models. However, the cuticle texture emerging on the surface of developing petal primordia cannot be predicted by our early theoretical model, which proposed that the final buckling outcome is simply a product of the rate of cuticle production and the extent and direction of epidermal cell expansion[13].

Our study reveals that the formation of ordered striations, and thus the production of structural colours, is strongly dependent on the chemical composition of the cuticle itself. We show that cuticular wrinkling in multiple *Hibiscus* species is associated with the presence of a high level of dihydroxy-palmitic acid and waxes and the exclusion (or reduced levels) of probable phenolic compounds. We have also demonstrated, using a transgenic approach in a new model system, that interfering with the production of these compounds can impair striation formation in *Hibiscus trionum* to various degrees, both during development or upon application of a mechanical force. Chemical changes such as these may alter the behaviour of the cuticle under compressive forces through changes in its material properties. For example, the viscosity of the cuticle (which may result from its degree of polymerisation and its relative wax and lipid content), its strength and its stiffness (or Young's modulus) may all be impacted. Previous studies have demonstrated the particular importance of relative stiffness in the wrinkling behaviour of layered systems [31–33]. The chemical composition of the cuticle could also affect its organisation, producing architectures that are more or less favourable to buckling. The relationship between cuticle chemical composition and its ultrastructure is not fully understood but the nature of the molecules delivered to the cell surface, as well as their timing and rate of delivery, are all likely to influence the layered organisation of the cuticular membrane [44]. More recent models than the one tested here propose that the cuticle of *Hibiscus* behaves as a bilayer with a relatively stiff thin film on a soft substrate [14,15]. The data reported here are compatible with this model, without testing it explicitly: the results of the mechanical perturbations suggest that a change in cuticle chemistry could be sufficient to change its buckling propensity. It will be interesting in future studies to investigate whether a change in cuticle chemistry is sufficient to trigger a change in the formation of a bilayered structure, or of its mechanical properties, or both. Such studies will be necessary to establish the exact contribution of chemistry to the resulting material properties of the cuticle, but our results show that flowering plants can control precisely the position and

size of diffraction gratings on their petals by specifying where distinct biosynthetic pathways are active across the epidermis. Floral diffraction gratings are pseudo-ordered, and the presence of disorder plays a key role in shifting the optical effect toward the blue/UV end of the spectrum visible to insect pollinators [11]. It remains to be established whether cuticle chemistry can also fine-tune cuticular mechanical properties with sufficient accuracy to control the regularity of the grating itself.

Acknowledgments

We thank Matthew Dorling for excellent plant care, Brian G. Murray and Doekele G. Stavenga for the generous gift of seeds and Ray Wightman, manager of the Imaging Core Facility at SLCU, for his help and expertise with the CryoSEM imaging and cryo-fractures. We acknowledge the collections at Cambridge University Botanic Garden and the Millenium Seed Bank at Wakehurst Place, Royal Botanic Gardens, Kew. **Funding:** This work was funded by EU Marie Curie actions (NanoPetals to E.M and B.J.G and I.T.N PlaMatSu (722842) to B.J.G), a BBSRC grant BB/P001157/1 to B.J.G and M.K, the European Research Council (ERC Consolidator Grant 279405 to M.K) and the Herchel Smith fund and the Gatsby Charitable Foundation to E.M.

Author contributions

EM and BJG designed the study; EM, CAA, JF, CG, SSS, MK, PJR, CJP, SH, JFW and SR performed the experiments and analysed the data as follows: EM isolated the different *H. trionum* genes, built the different plant expression vectors and developed the transformation protocol for *H. trionum*; EM and CAA produced, imaged and analysed the transgenic *Hibiscus* lines; EM, SH, CAA and JF measured cell expansion and cuticle thickness; CAA performed and analysed the qPCR experiments; CJP and PJR performed and imaged the FatRed staining of the cuticle; CG and SSS performed the LESA-MS analyses, and analysed the data with MK; JFW performed the phylogenetic analyses; JF performed the PCA analyses; SR and EM performed the mechanical perturbation experiments, EM prepared the figures and wrote the manuscript with BJG. All authors read and commented on successive drafts of the manuscript and approved the final version.

Declaration of interests

BJG is a member of the Advisory Board of Current Biology. The authors declare no other competing interests.

Inclusion and Diversity

We support inclusive, diverse, and equitable conduct of research.

Main Figures

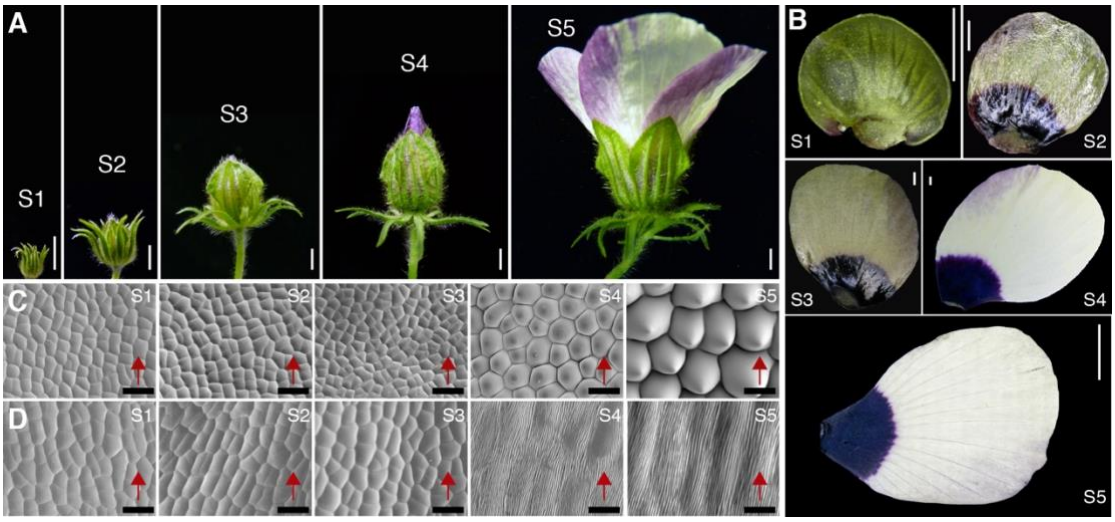

Figure 1. Diffraction gratings emerge halfway through bud development and are restricted to the petal base surface in *H. trionum*.

Stereotypical stages of *H. trionum* bud development (S1-S5). S5 is the mature open flower. At S4, petal tips become visible. At S3, the crown of bracts opens and bends towards the horizontal. At S2 pigmentation appears on the petal adaxial epidermis, dividing the petal surface between an anthocyanin-rich proximal region and a non-pigmented distal region. S1 petals are entirely green. (**A**) Representative images of a bud at each stage, scale bars = 0.5 cm. (**B**-**D**) Representative images of a dissected petal at each stage, adaxial epidermis visible, scale bars = 1 mm in S1-S4; scale bar = 1 cm in S5. SEM images showing cells in the distal (**C**) or proximal (**D**) region of the adaxial petal epidermis at each stage, scale bars = 20 μm. Differences in cell shape and cuticular patterning appear between S3 and S4. Red arrows indicate the base-to-tip axis of the petal.

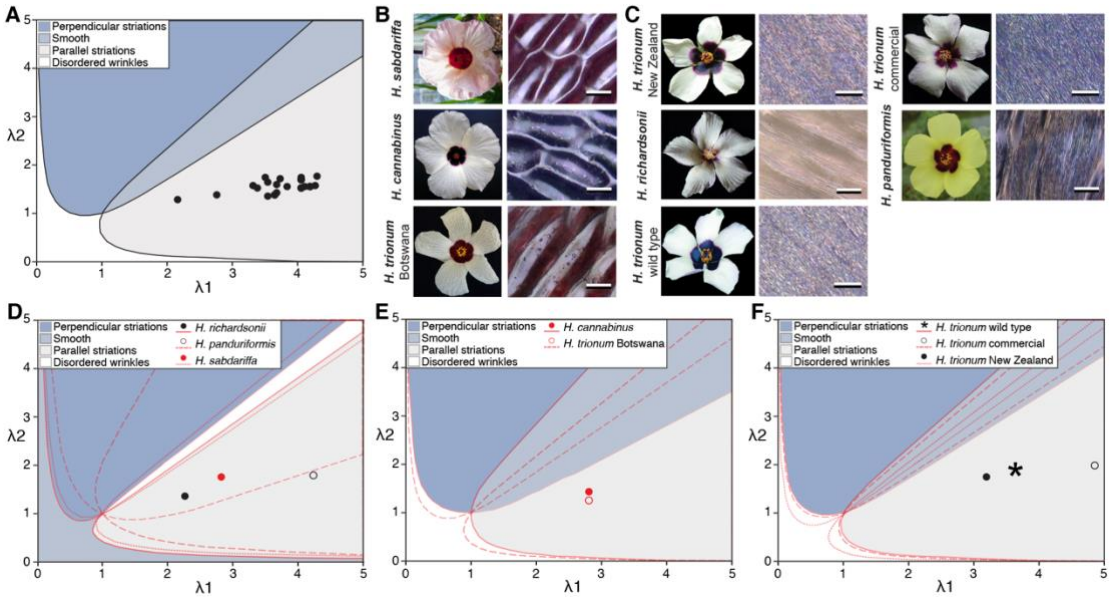

500 **Figure 2. Cell growth and change in cuticle thickness are insufficient to predict cuticular pattern.**

502

(**A**) Model prediction of cuticular pattern according to Antoniou-Kourounioti *et al.* [13], 504 with cuticle production rate ß = 0.85 and λ_1 and λ_2 representing expansion parallel and perpendicular to the long axis of the tabular cells. See Figure S1 H-J. The pattern 506 expected in each subregion of the graph is given in the key. Each black circle corresponds to average cell measurements (cells measured ≥ 20 per petal, for ≥ 5 508 petals) in the proximal petal region of flowers treated with plant hormones (IAA, GA3) or drugs known to interfere with cell growth (NPA, orizalin, taxol). **B**) Left: 510 representative flowers from three *Hibiscus* species displaying a smooth cuticle in the proximal (pigmented) region of the petal adaxial epidermis. Right: close-up image of 512 smooth surface cells from the proximal region, scale bar = 30 μm. (**C**) Left: representative flowers from five *Hibiscus* species displaying a striated cuticle in the 514 proximal (pigmented) region of the petal adaxial epidermis. Right: close-up image of striated cells from the proximal region, scale bar = 30 μm. (**D**) Model prediction of 516 cuticular pattern as in (A) but with ß = 1.05 (solid lines) for *H. richardsonii* (solid black circle), ß = 2.23 (dashed lines) for *H. panduriformis* (hollow black circle) and ß 518 = 1.09 (doted lines) for *H. sabdariffa* (solid red circle). (**E**) Model prediction of cuticular pattern as in (A) but with ß = 0.70 (solid lines) for *H. cannabinus* (solid red 520 circle) and ß = 0.92 (dashed lines) for *H. trionum* Botswana (hollow red circle). (**F**) Model prediction of cuticular pattern as in (A) but with ß = 0.85 (solid lines) for *H.* 522 *trionum* wild type (black asterisk), ß = 0.89 (dashed lines) for *H. trionum* commercial variety (hollow black circle) and ß = 0.97 (dotted lines) for *H. trionum* New Zealand 524 (solid black circle). Red indicates discrepancy between observed and predicted patterns.

526 See Also Figure S1, Table S1 and Data S1.

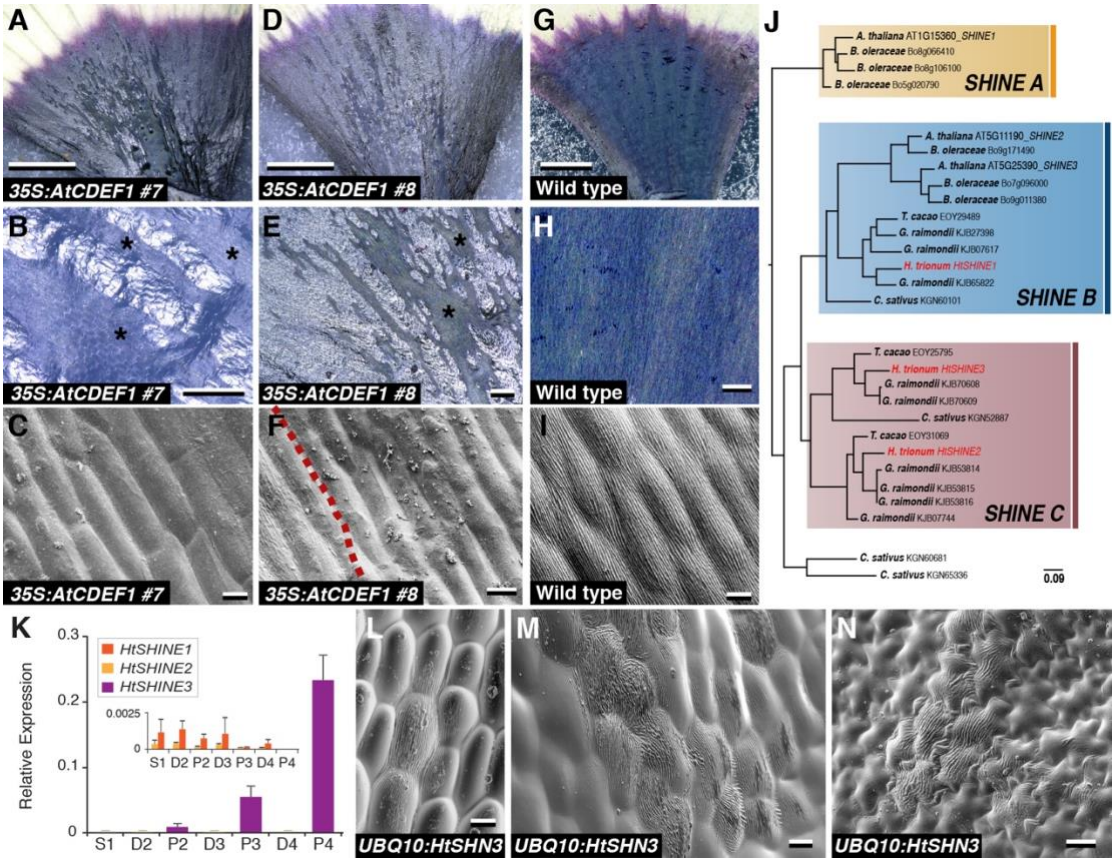

Figure 3. Modifying cuticle production is sufficient to interfere with cuticle patterning.

(**A-C**) *H. trionum 35S:AtCDEF1* transgenic line #7 or (**D-F**) line #8. (**G-I**) *H. trionum* wild type. (**A**, **D**, **G**) Light micrographs of the adaxial petal epidermis proximal region. The blue shine in wild type is mostly absent in *35S:AtCDEF1* lines (**B**, **E**, **H**) close-up view of the proximal region of the adaxial petal epidermis. The epidermis of *35S:AtCDEF1* show patches of striated (*) and smooth cells while cells are always striated in wild type. (**C**, **F**, **I**) SEM imaging of adaxial epidermis cells from the proximal region. Cells from C and F located in one of the smooth patches observed in B or E, respectively, lack striations while the neighbouring cells located in a striated region (below the red dotted line in F) display faint striations. Cells from equivalent regions in wild type (I) are all covered with prominent cuticular striations. (**J**) Phylogenetic analysis of the *SHINE* clade in Brassicales-Malvales (Malvaceae: *G. raimondii*, *T. cacao* and *H. trionum*); Brassicaceae: *A. thaliana*, *B. oleracea*) reveals 3 major subgroups. Another rosid, *C. sativus* (Cucurbitales), is used as outgroup. See also Data S2 (**K**) Relative expression of *HtSHINE* genes in developing petals of *H. trionum* wild type, see Figure 1 for stages. Error bars represent standard deviation (**L-N**) SEM imaging of the petal epidermis in flowers from *PromUBQ10:HtSHINE3* line. (**L**) Ectopic striations are visible on the surface of some cells located in the bullseye boundary region on the adaxial petal epidermis. Ectopic striations also develop in the proximal (**M**) and distal (**N**) regions on the abaxial epidermis. The abaxial epidermis and the adaxial boundary region are completely smooth in wild type (Figure S3B-D). Scale bar, 2.5 mm (A, D and G), 200 μm (B, E and H), 20 μm (C, F and I), and 10 μm (L-N).

See also Figures S2, S3 and Data S2.

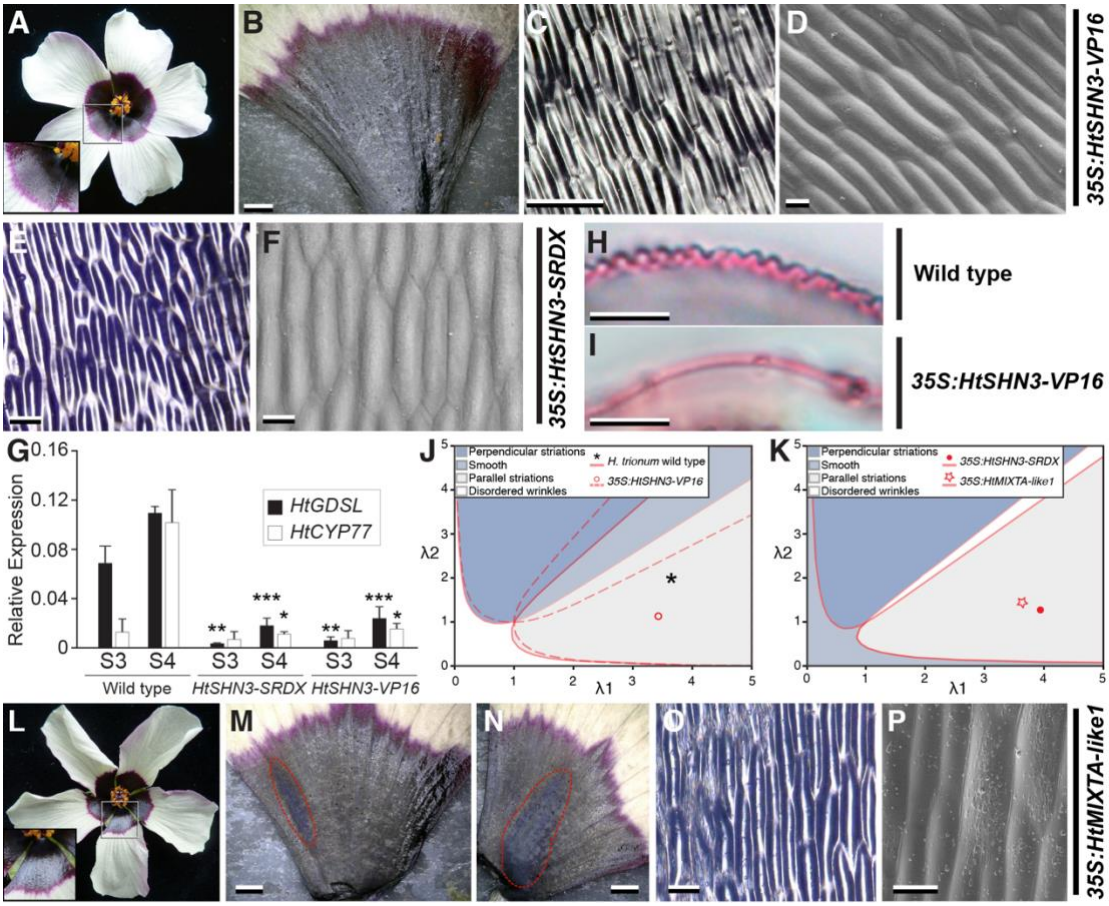

Figure 4. Cuticular striations can be lost without changing cell shape or cuticle thickness.

(**A**-**D**) Floral phenotype of *5S:HtSHN3-VP16 H. trionum* transgenic lines (**A**) Representative flower showing the absence of blue sheen in the flower centre. (**B**) Close-up view of the proximal region of the adaxial petal epidermis. (**C**) Light and (**D**) SEM imaging of cells from the epidermis region shown in (B). Striations are absent and cells are smooth. (**E**-**F**) Floral phenotype of *35S:HtSHN3-SRDX H. trionum* transgenic lines (**E**) Light imaging and (**F**) SEM imaging of the cells from the proximal region of the adaxial petal epidermis. Striations are absent and cells are smooth. (**G**) Relative expression levels of *HtGDSL* and *HtCYP77* in the proximal region of developing petals of *H. trionum* wild type, *35S:HtSHN3-SRDX*, and *35S:HtSHN3-VP16* at S3 and S4. * $p < 0.05$, ** $p < 0.02$ and *** $p < 0.001$, Welch's *t*-test. Error bars represent standard deviation. (**H**) Light imaging of cross-sections of petal epidermis (adaxial proximal region) from *H. trionum* wild type and (**I**) *35S:HtSHN3-VP16* transgenic line stained with FatRed. The cuticle appears pink. (**J**) Model prediction of cuticular pattern as in Figure 1 with ß = 0.85 (solid lines) for *H. trionum* wild type (black asterisk), ß = 0.685 (dashed lines) for *35S:HtSHN3-VP16* (hollow red circle) and (**K**) ß = 1.05 for *35S:HtSHN3-SRDX* (solid red circle) and *35S:HtMIXTA-like1* (hollow red star). Red indicates discrepancy between observed and predicted patterns. (**L**-**P**) *H. trionum* transgenic lines constitutively expressing *HtMIXTA-like1* (*35S:HtMIXTA-like1*). (**L**) Representative flower (line #1) showing the lack of blue sheen in the flower centre. (**M**-**N**) Close-up view of the proximal region of the adaxial petal epidermis from line #1 and #2, respectively. A blue patch

(dotted red line) coincides with residual striations. The images represent the two extremes in terms of size of the striated patch. (**O**) Light and (**P**) SEM imaging of epidermis cells from the region shown in (M). Most cells have a smooth cuticle, but residual faint striations are visible on some cells on the left. Scale bar, 2 mm (B, M, and N), 100 μm (C), 25 μm (D and F), 40 μm (E and P), 5 μm (H and I), and 50 μm (O).

See also Figures S1, S2, S4 and S6 and Table S1.

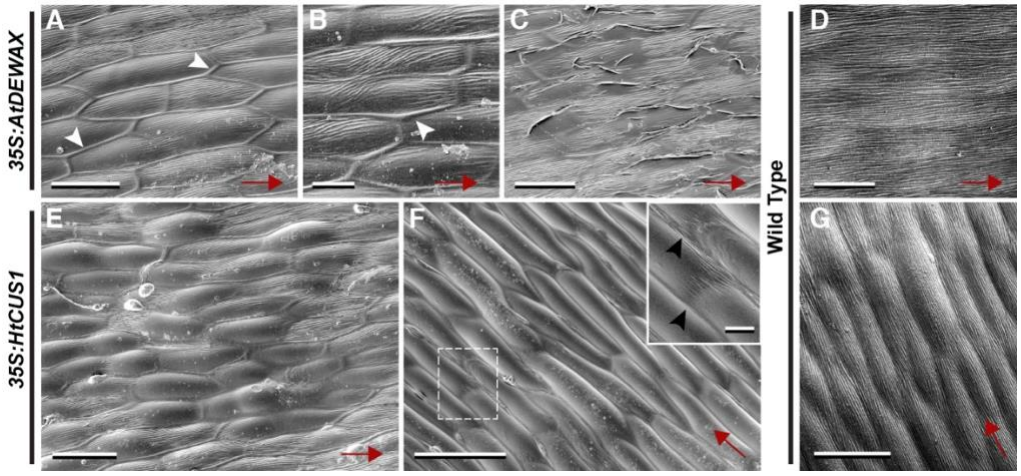

Figure 5. Diffraction grating formation is impaired when genes controlling cutin assembly and cuticular wax synthesis are misexpressed.

(**A-D**) SEM imaging of (A-C) proximal region of *35S:AtDEWAX H. trionum* adaxial petal epidermis and (D) equivalent region in wild type. Cuticular striations are present but faint (A) and disorganised (B) or severely disrupted (C). The cuticle accumulates abnormally at the junction between neighbouring cells (white arrowhead). (**E-G**) SEM imaging of (E-F) the proximal region of *HtCUS1 H. trionum* adaxial petal epidermis and (G) equivalent region in wild type. Cuticular striations are frequently absent and, when present they are faint (E) and interrupted, or very short (F) and only found at the junction between neighbouring cells (black arrowheads). Scale bar, 50 μm (A and C-G), 20 μm (B), and 10 μm (close-up view in F). Red arrows indicate the base-to-tip axis of the petal.
See also Figures S2 and S5.

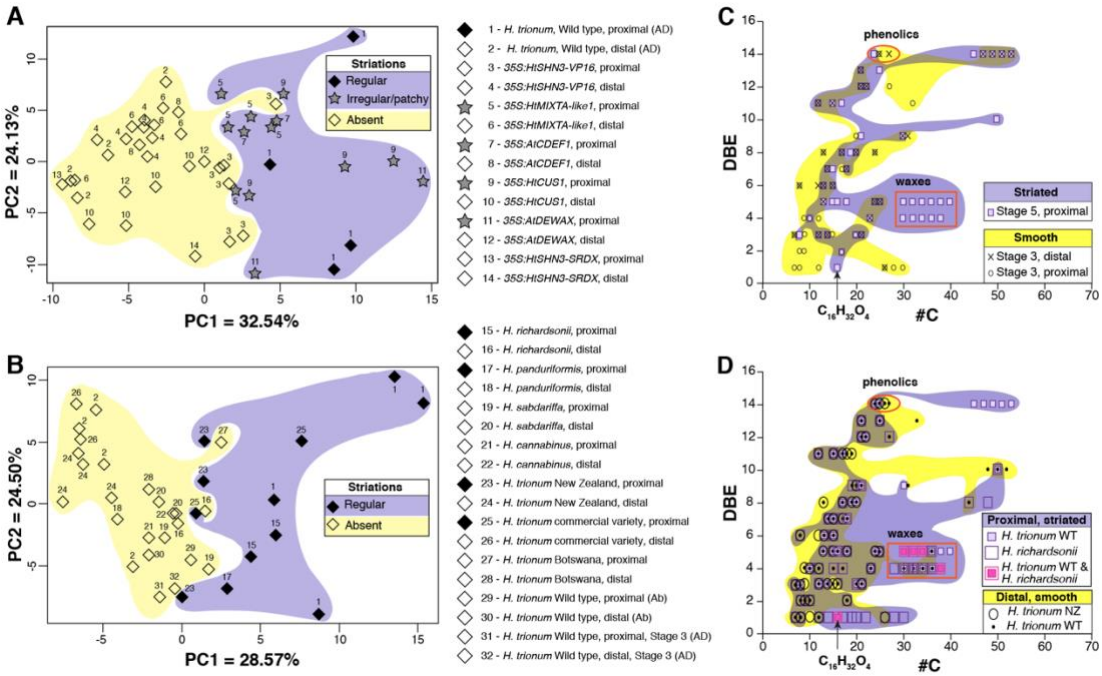

608

Figure 6. Striated cuticles share a common chemical profile.

610

(**A**) Principal component analyses of cuticle chemical composition characterised by
612 LESA-MS of wild type and transgenic lines of *H. trionum* or (**B**) of *H. trionum* and related species from Figure 2B-C. Each sample type is represented by a symbol with a
614 number. The number indicates the species/line and petal region analysed and the symbol indicates whether the sample surface is striated or smooth. Samples 1 and 2
616 are identical, included in both analyses for reference. In each plot, regions occupied by smooth and striated samples are shaded with yellow and purple, respectively (**C**
618 and **D**) Comparison between the chemical composition (shortlisted compounds only, plotted according to Double Bond Equivalent (DBE) vs. the number of carbons (#C))
620 of (**C**) the smooth surface of petal primordia (S3, proximal and distal regions) and the striated surface of open flower petals (S5, proximal region) or (**D**) striated and smooth
622 petal surfaces in open flowers from different species or populations. Symbols corresponding to compounds detected on the surface of both types of striated cuticles,
624 and only there, have been coloured pink. The regions of the plot occupied by smooth and striated samples are shaded in yellow and purple, respectively (overlap appears
626 brown).
See also Table S2, Data S1 and S4.

628

STAR Methods

RESOURCE AVAILABILITY

Lead contact

Further information and requests for resources should be directed to and will be fulfilled by the lead contact, Edwige Moyroud (em500@cam.ac.uk)

Materials availability

Plasmids used to generate transgenic plant material are available upon request. Seeds from fertile transgenic lines harbouring T-DNAs from those plasmids are available upon request. This study generated no other new unique reagents.

Data and code availability

- The accession numbers of the sequenced genes reported in this paper are GenBank: MW801437, GenBank: MW801438, GenBank: MW801439, GenBank: MW801440 and GenBank: MW801441). The Phylogenetic tree for AP2/ERF can be found in Data S2. Primers are listed in Data S3. The frequency of detection for each of the 135 compounds used for a target compound search in all Hibiscus samples (wild type and transgenic lines of *H. trionum* and various other Hibiscus species) following LESA-MS analyses are provided in Data S4.
- This paper does not report original code and all software and algorithms are available from the references listed in the Key Resources Table.
- Any additional information required to reanalyze the data reported in this paper is available from the lead contact upon request.

EXPERIMENTAL MODEL AND SUBJECT DETAILS

Plant material and growth conditions

Plants were grown under glasshouse conditions on a 16 hours of light, 8h of dark photoperiod at 23 °C, minimum radiance 405 µmol.m^{-2}.s^{-1}, in Levington's M3 (UK) compost using *H. trionum* L. seeds (*H. trionum*, wild type) and *H. sabdariffa* seeds from Chiltern seeds (UK); *H. panduriformis* form Sunshine seeds (Germany) or *H. cannabinus* seeds purchased from Jungle seeds (UK). *H. trionum* commercial seeds from [45] were supplied Doekele G. Stavenga. *H. richardsonii* (Mayor Island (Tuhua),

New Zealand - Voucher AK251841) and *H. trionum* New Zealand 'naturalised race' (Bream Head, North Island, New Zealand - Voucher AK253689) were supplied by Brian G. Murray [46]. Seeds from *H. trionum*, Botswana were obtained from the Millennium Seed Bank (Accession number 91154). Plants received supplemental lighting from Osram 400 W high-pressure sodium lamps (Osram, München, Germany) during the growth period.

METHOD DETAILS

Plant Tissue collection

Petal tissues were harvested from developing buds (stage 1-5), between 9:00 am and 11:00 am when stage 5 flowers are fully open. Petals from stage 2 to 5 were dissected to separate the proximal region (purple) from the distal region (white) and immediately frozen in liquid nitrogen. Leaves and Stage 1 petals were frozen in liquid nitrogen without any dissection. All tissue samples were stored at -80 °C until RNA extraction.

Gene isolation

The full-length coding sequences of *HtSHINE1*, *HtSHINE2*, *HtSHINE3*, *HtMIXTA-like1* and *HtCUS1* were isolated from *H. trionum* mixed buds cDNA, using a combination of PCR with degenerate primers, 3' RACE and CELI-PCR [47]. Degenerate primers (Data S3) were designed to match regions conserved between homologs from cotton (*Gossypium raimondii*) and cocoa (*Theobroma cacao*), two Malvaceae species whose sequenced genomes can be freely accessed via Phytozome v11.0. The full-length coding sequences of *AtDEWAX* (*At5G61590*) and *AtCDEF1* (*At4G30140*) were amplified by PCR from *A. thaliana* (Col-0) bud and leaf cDNA. The corresponding sequences have been deposited in GenBank under the following accession numbers: *HtSHINE1* (MW801439), *HtSHINE2* (MW801440), *HtSHINE3* (MW801441), *HtMIXTA-like1* (MW801437) and *HtCUS1* (MW801438).

Construction of plant expression vectors

The coding sequence of *AtCDEF1* was amplified by PCR using Phusion® High-Fidelity DNA Polymerase and primers oEM234F x oEM235R (Data S3). The PCR product was cloned in the pBluescript KS(-) vector backbone using the EcoRV site to generate the intermediate vector pEM111. Traditional cloning following restriction

digest by EcoRI was used to extract the coding sequence of *AtCDEF1* from pEM111 and insert it into a modified pGREEN II vector backbone containing a double 35S promoter driving transgene expression, yielding the plant expression vector pEM112. The coding sequences of all other genes used to generate transgenic lines were amplified by PCR using Phusion® High-Fidelity DNA Polymerase and primers oEM113F x oEM114R (*HtSHINE3*), oEM186F x oEM187R (*AtDEWAX*), oEM198F x oEM199R (*HtCUS1*), oEM220F x oEM221R (*HtMIXTA-like1*). Gibson assembly [48] was then used to insert the coding sequence of *HtSHN3* into a modified pGREEN II vector backbone containing the promoter region of *AtUBIQUITIN10* (*PromUBQ10*), yielding the plant expression vector pEM76; or to insert the coding sequence of *AtDEWAX*, *HtCUS1* or *HtMIXTA-like1* into a modified pGREEN II vector backbone containing a double 35S promoter, yielding the plant expression vectors pEM98, pEM100 and pEM109, respectively. Gibson assembly was also used to fuse the coding sequence of *HtSHN3* with the sequence coding for the SRDX domain (using primers oEM242F x oEM243R) or with the VP16 domain (using primers oEM168 to oEM171) and produce the plant expression vectors pEM115 and pEM114, respectively (Data S3). The integrity of all plant expression vectors was verified using Sanger sequencing carried out on an Applied Biosystems 3730xl DNA Analyser (Biochemistry DNA Sequencing Facility, University of Cambridge, UK) prior to plant transformation.

Plant transformation

A protocol to generate transgenic *H. trionum* plants was developed using Agrobacterium-mediated transgene delivery followed by tissue culture to induce callus production and plant regeneration.

Agrobacterium *transformation*

Electrocompetent *Agrobacterium tumefaciens LBA4404* cells were transformed with plant expression vectors pEM76 (*PromAtUBQ10:HtSHINE3*), pEM98 (*35S:AtDEWAX*), pEM100 (*35S:HtCUS1*), pEM109 (*35S:HtMIXTA-like1*), pEM112 (*35S:AtCDEF1*), pEM114 (*35S:HtSHN3-VP16*) or pEM115 (*35S:HtSHN3-SRDX*). Transformed cells were selected on LB agar plates containing 50 $mg.L^{-1}$ Kanamycin and 25 $mg.L^{-1}$ streptomycin after 48 hours incubation in the dark at 30 ˚C.

H. trionum *infection and regeneration*

On day 1, *H. trionum* seeds were sterilised by incubation for 5 min in 70% (v/v) EtOH + 10% (w/v) SDS, followed by 1 min in 95% (v/v) EtOH, and a ddH2O rinse. Dormancy was then disrupted by incubating the seeds for 10 min in 90 ℃ ddH2O. The sterilised seeds were transferred onto germination media [2.2 g MS salts with vitamins (Duchefa), 25 g sucrose, 6 g Plant agar (Sigma), up to 1 L ddH2O, pH 5.7] and incubated for 36 h in the dark at 30 °C. In parallel, an *Agrobacterium* preculture was started by incubating a colony containing the plant expression vector in 5 mL LB with 50 $mg.L^{-1}$ kanamycin and 25 $mg.L^{-1}$ streptomycin at 28 ˚C, 220 rpm, overnight. Two larger cultures were prepared the following day (day 2), using 50 mL LB supplemented with 50 $mg.L^{-1}$ kanamycin, 25 $mg.L^{-1}$ streptomycin and 50 µL or 500 µL *Agrobacterium* preculture. These cultures were incubated overnight at 28 ˚C, 220 rpm. On day 3, following overnight incubation, the two cultures were pooled and centrifuged for 10 min at 4,000 rpm. The pellet was re-suspended in 20 mL induction solution [2.2 g MS salts with vitamins (Duchefa), 30 g sucrose, 0.2 mM acetosyringone (Sigma), up to 1 L ddH2O, pH 5.7] and incubated for one hour at 28 ˚C, 220 rpm. The germinated seeds were dissected under a sterile air hood and the roots, shoot apical meristems and cotyledons were discarded. The hypocotyls were cut into ~0.5 cm long sections and incubated with the *Agrobacterium* culture for 10 minutes before rinsing and plating on MS Hib plates [4.4 g MS salts with vitamins (Duchefa), 35 g sucrose, 40 $mg.L^{-1}$ cysteine (Sigma), 15 mg ascorbic acid (Sigma), 8 g Plant agar (Sigma), up to 1 L ddH2O, pH 5.7) containing 0.01 $mg.L^{-1}$ TDZ, 0.05 $mg.L^{-1}$ BA and 0.2 mM acetosyringone (Sigma). Plates were kept in the dark at room temperature for 48 hours. On day 5, hypocotyls were moved to fresh MS Hib plates containing 0.01 $mg.L^{-1}$ TDZ, 0.05 $mg.L^{-1}$ BA, 250 $mg.L^{-1}$ cefotaxime and 150 $mg.L^{-1}$ kanamycin, and plates were transferred to a tissue culture room at 24 °C, 16 hours light, 391 $\mu mol.m^{-2}.s^{-1}$ illumination. On day 12 and day 19, the hypocotyls were transferred to new MS Hib plates containing 0.2 $mg.L^{-1}$ BA, 250 $mg.L^{-1}$ cefotaxime and 150 $mg.L^{-1}$ kanamycin. From day 33 onwards, calli were moved every 7-10 days to fresh MS Hib plates containing 250 $mg.L^{-1}$ cefotaxime and 150 $mg.L^{-1}$ kanamycin. Calli and regenerating plantlets were assessed weekly under a V12 stereo fluorescence microscope (Zeiss) to check whether the transformation was successful (transformed cells expressing a fluorescent eYFP protein). Once transformed regenerated plantlets were ~ 1 cm tall, those were cut and transferred to 100 mL

762 sterile Hamilton jars containing 30 mL rooting media [2.2 g MS salts with vitamins (Duchefa), 25 g sucrose, 6 g Plant Agar (Sigma), up to 1 L ddH2O, pH 5.7). Once
764 roots had developed, regenerated plants were transferred to Levington's M3 (UK) compost and moved to the greenhouse.
766

Gene expression analysis

768 Frozen tissues were ground to a fine powder using mortar and pestle. RNA was extracted using SIGMA Aldrich Spectrum Plant Total RNA kit and retro-transcribed
770 with Invitrogen SuperScriptII following the manufacturer's instructions. Quantitative real time PCR was performed using a Biorad CFX6 PCR machine and Luna Universal
772 qPCR Master Mix (New England Biolabs). *HtActin* was chosen as a housekeeping gene after testing 5 candidate housekeeping genes across different stages and across
774 biological replicas. The primer efficiencies were 95% for *HtActin*, 100% for *HtSHN3* primers, 105% *HtSHN1*, 104% *HtSHN2*, 97% for *HtCUS1*, 99% for *HtMIXTA-like1*,
776 95% for *AtCDEF1*, 94% for *HtGDSL*, 98% for *HtCYP77*. Primer sequences are given in Data S3. The gene expression was calculated relative to the housekeeping gene
778 actin and the common base method, which accounts for the measured efficiency of each primer pair, was used to calculate relative expression levels [49]. Welch's *t*-tests
780 were used to test for the likelihood that transgenic lines and wild type in Figure 4I had the same average expression levels in equivalent petal tissues. RT-PCR was
782 performed by retrotranscribing RNA from leaves of transgenic plants, using SuperScript™ II (Invitrogen). Manufactured cDNAs were then used as template for
784 the PCR reaction, performed using PCRBIO (PCR Biosystems). The sequences of primers used are given in Data S3. 5 µL of the RT-PCR product were collected after
786 23, 28 and 35 cycles and run on an agarose gel.

788 ***Phenotyping***

H. trionum wild type buds at various stages of development and open flowers from
790 different *Hibiscus* species and *H. trionum* transgenic lines were placed on black velvet and imaged with a Panasonic Lumix DMC-L10 Camera. Dissected petals of *H.*
792 *trionum* wild type and transgenic lines or from different *Hibiscus* species were imaged either on black velvet with a Panasonic Lumix DMC-L10 Camera (full petal) or on a
794 black stage with a Keyence VHX5000 microscope and a Z1000 lens (close-up imaging).

796

CryoSEM imaging and Cryo-fractures

798 The petal surfaces from *H. trionum* wild type or transgenic lines were imaged using a Hitachi S-4700 Cryo-SEM and a Zeiss-Quorum Cryo-SEM. For each sample, about
800 $10mm^2$ of tissue was mounted on a stage, fixed by cooling in nitrogen slush, before being sputter-coated with gold or platinum in the antechamber of the SEM and
802 introduced into the main chamber to be imaged. Cryo-fractures were performed as described in [15] with the following modifications: following cryofracture, samples
804 were sputter coated with 8 nm Platinum and imaging was carried out on a Zeiss EVO HD SEM using 6 kV gun voltage and 16 pA probe current.

806

Cuticle staining and thickness measurements

808 Stage 3 buds and Stage 5 open flowers were collected from wild type and transgenic lines of *H. trionum*. Following petal dissection, 2 mm^2 sections of petal tissue were
810 excised from the proximal region of the petal using a mounted needle and fixed in 2.5% (v/v) glutaraldehyde in phosphate buffer pH 7.4 at 4 °C for 48 hours. For Fat
812 Red staining, a saturated solution (0.3 g of stain in 20 mL of ethanol) of Sudan Red 7B in 100% ethanol was used. Samples were washed four times (30 min at 4 °C) in
814 0.05 M phosphate buffer pH 7.4 before being dehydrated to 100% ethanol at room temperature, then transferred into the prepared stain for one hour. Sections were cut
816 directly into 100% glycerol and then imaged with a Leica LMD7000 photomicroscope. Cuticle thickness was measured using ImageJ from pictures taken
818 with the Leica LMD7000 photomicroscope. At least 50 measurements were done for each sample and used to estimate the mean cuticle thickness. For each genotype, β
820 was calculated as the ratio 'mean cuticle thickness at stage 5 (after cell growth)': 'mean cuticle thickness at stage 3 (before cell growth)', according to [13]. An
822 illustration of these measurements and ratio calculations is provided in Figure S1H-J.

824 ***Drug and hormone treatments***

Lanolin containing different concentrations (10 μM, 30 μM, 50 μM, 100 μM or 1
826 mM) of IAA (Sigma), gibberellic acid (Fischer scientific), NPA (Sigma), Taxol (Sigma) or Oryzalin (Sigma) was applied to the base of *H. trionum* Stage 3 buds.
828 Alternatively, a water-based solution of IAA and NPA (10 μM to 100 μM) was injected between the sepals and petals of stage 3 *H. trionum* buds using a syringe and

needle. In all cases, buds were allowed to develop fully to stage 5 on the plant. Open flowers were collected on the day of flowering and the proximal region of the adaxial petal surface was imaged using a Keyence VHX 5000 microscope (Z100 and Z1000 lenses).

Cell expansion measurements

Cell sizes were measured with ImageJ from pictures taken with a Keyence VHX5000 microscope and a Leica M205FA stereomicroscope using epi- or transmitted illumination. At least 20 cells were measured for each sample and used to estimate the mean cell length (parallel to the proximo-distal axis of the petal) and mean cell width (perpendicular to the proximo-distal axis of the petal). Expansion λ_1 and λ_2 were defined as the ratios 'mean cell length at stage 5 (after cell expansion)': 'mean cell length at stage 3 (before cell growth)' and 'mean cell width at stage 5 (after cell expansion)': 'mean cell width at stage 3 (before cell growth)', according to [13]. An illustration of these measurements and ratio calculations is provided in Figure S1H-J.

LESA-MS analysis of cuticle chemistry

LESA-MS analyses of spatially resolved cuticle chemical composition were performed according to the method described in detail in [34]. Specifically, after harvest the flowers were kept in the fridge in the dark and the petals were analysed within 2-3 days. Petals were removed from the flowers using tweezers, placed flattened on the LESA plate and cleaned with a nylon brush under a gentle stream of nitrogen to remove pollen residues. Each sample was analysed for spatially resolved chemical composition with two different solvents: a polar mixture of water with 0.1% (v/v) of formic acid/acetonitrile (10:90) and an apolar mixture of acetonitrile/chloroform/water with 0.1% (v/v) formic acid (49:49:2). At least three analyses were conducted for each portion (proximal vs distal) of the petal for each solvent, and at least three different petals for each sample type were analysed. For each individual analysis, a droplet of 3 µL of solvent was deposited by a conductive pipette tip at a height of 1.4 mm from the sample plate at the maximum dispensation rate (60 $\mu L.min^{-1}$). The liquid junction between the pipette tip and the petal surface was maintained for 30 s for the nonpolar mixture and for 45 s for the polar mixture. The droplet containing the dissolved analytes was then aspirated back into the tip at a height of 1.2 mm from the sample plate at the maximum aspiration rate (60 $\mu L.min^{-1}$)

and infused in a chip-based nanoESI source (Triversa NanoMate Advion, Ithaca, NY, USA). Samples were sprayed at a gas (N2) pressure of 0.80 psi at −1.4 kV in negative ionization mode with a transfer capillary temperature of 210 °C. Blanks were analysed by repeating the same procedure on the clean aluminium foil placed underneath the petals, with a dispensation height of 1.2 mm and an aspiration height of 1.0 mm from the surface. Mass spectrometry analysis was performed using an LTQ Velos Orbitrap mass spectrometer (Thermo Scientific, Bremen, Germany) with a resolution of 100 000 at m/z 400 and a typical mass accuracy within ±2 ppm. Data was acquired using an automated acquisition method to record the full scan in the m/z ranges 80−600 and 150−1000. Additional details on the chemical analysis and data processing can be found in [34] and in [50]. For the Principal Component Analysis (PCA), compounds that were reliably detected across equivalent samples corresponding either to the smooth or the striated portions of wild type *H. trionum* petals were selected from the LESA-MS analysis. This yielded a list of 135 compounds that were then used for a target compound search in all other samples (*H. trionum* transgenic lines and other wild *Hibiscus* species, Data S4). The 'ade4' package [51] from R [52] was used to perform the PCAs.

Phylogeny reconstruction

Coding sequence data for *Arabidopsis thaliana*, *Theobroma cacao*, *Brassica oleracea*, *Gossypium raimondii* and the outgroup *Cucumis sativus* were downloaded from Ensembl Plants (12/03/2019; release-42). Initial homology was determined using BLASTP [53] with the settings "-max_target_seqs 200 -evalue 1e-3". This was conducted on a database containing all amino acid coding sequences from the genomes and the translated *HtSHN* sequences were used as a query. The corresponding nucleotide sequence for every blast hit was extracted and combined with the *HtSHN* nucleotide sequences. The sequences were aligned using MAFFT v7.271 [54] , with the settings "--auto --maxiterate 1000". The alignment was cleaned for a minimum of 10% column occupancy using phyx v.0.999 [55], and model selection was conducted using the ModelFinder [56] test as implemented in IQtree v1.6.3 [57]. A maximum likelihood tree was inferred under the general time reversible model, with empirical base frequencies, and a gamma distribution with nine rate categories using IQtree v1.6.3 [57], with 1000 ultrafast bootstraps [58] conducted for support.

Mechanical perturbations

As in Airoldi *et al*. (2021) [15] mechanical stress was applied to the petals using an adapted automated confocal micro-extensometer [59]. The extensometer was constructed using a 50 g force sensor (Futek LSB200), and a Smaract, SLC-1740 - Linear Piezo Stage. To enable visualization of the striations the extensometer was coupled to a Keyence VHX-5000 microscope with a 500-X objective. To avoid dehydration the sample was floated on an isotonic solution of 0.2 M NaCl. Strips of petal were attached to the extensometer using tough-tags (0.94 × 0.50 inches, distal (white), catalogue no. TTSW-1000; DiversifiedBiotech) and cyanoacrylate super glue. The sample was subjected to 60-65 mN of tensile stress. Images were taken of the sample at 2000x zoom before and after the experiment.

QUANTIFICATION AND STATISTICAL ANALYSIS

For statistical analysis, Welch's t-test or ANOVA followed by Tukey's HSD post-hoc test were used to assess significant differences between the samples using the statistical software R (https://www.r-project.org). The PCA analyses were performed using the 'ade4' package [51] from R [52]. Cell dimensions were quantified using ImageJ (https://imagej.nih.gov/ij/). For each quantification performed, the value of n and what n represents is provided in the Methods Details, the Results and/or the legends of the figures and tables. Following LESA-MS analysis, molecular formulas were assigned using Xcalibur 2.1 (Thermo Scientific, Bremen, Germany) and data were then filtered using a Mathematica 10 (Wolfram Research Inc., UK) code already described in [34].

KEY RESOURCES TABLE

Supplemental data titles and legends

Data S1. Phylogenetic placement of the different Hibiscus species used in this study, Related to Figure 2 and Figure 6. Simplified phylogeny of the Hibiscus genus. The relationships between the six main clades are represented, according to [S2]. The five different species used in this study belong to the Trionum and Phylloglandula sections.

Data S2. Phylogenetic reconstruction of the AP2/ERF family, Related to Figure 3. This includes all AP2/ERF genes from *Arabidopsis thaliana*, *Brassica oleracea*, *Cucumis sativus*, *Gossypium raimondii* and *Theobroma cacao*. It also includes the three *HtSHINE* genes from *Hibiscus trionum*. The section of the phylogeny corresponding to the *SHINE* subgroup represented in Figure 3J is boxed. Specific genes functionally characterised in Arabidopsis and groups identified by [S3] are also indicated on the right.

Data S3. List of primers used in this study, Related to STAR Methods. First tab = primer sequences used to isolate and clone genes; Second tab = primers used to build plant expression vectors; Third tab = primers used for qRT-PCR and RT-PCR.

Data S4. Frequency of detection for each of the 135 compounds used for a target compound search in all Hibiscus samples, Related to Figure 6. The numbers indicate the percentages of analyses performed on a given flower that detected each specific compound. At least three analyses were conducted for each portion (proximal vs distal) of the petal and at least three different petals for each sample type were analysed. Sample types include wild type *H. trionum*, transgenic lines of *H. trionum* and the various other Hibiscus species depicted in Figure 2.

References

1. Vukusic, P., and Sambles, J.R. (2003). Photonic structures in biology. Nature *424*, 852–855.
2. Burg, S.L., and Parnell, A.J. (2018). Self-assembling structural colour in nature. J. Phys. Condens. Matter *30*, 413001.
3. van der Kooi, C.J., Elzenga, J.T.M., Staal, M., and Stavenga, D.G. (2016). How to colour a flower: on the optical principles of flower coloration. Proc. R. Soc. B Biol. Sci. *283*, 20160429.
4. Vukusic, P., and Stavenga, D. g (2009). Physical methods for investigating structural colours in biological systems. J. R. Soc. Interface *6*, S133–S148.
5. Vignolini, S., Moyroud, E., Glover, B.J., and Steiner, U. (2013). Analysing photonic structures in plants. J. R. Soc. Interface *10*, 20130394.

6. Starkey, T., and Vukusic, P. (2013). Light manipulation principles in biological photonic systems. Nanophotonics *2*, 289–307.

7. Airoldi, C.A., Ferria, J., and Glover, B.J. (2019). The cellular and genetic basis of structural colour in plants. Curr. Opin. Plant Biol. *47*, 81–87.

8. Vignolini, S., Rudall, P.J., Rowland, A.V., Reed, A., Moyroud, E., Faden, R.B., Baumberg, J.J., Glover, B.J., and Steiner, U. (2012). Pointillist structural color in Pollia fruit. Proc. Natl. Acad. Sci. *109*, 15712–15715.

9. Middleton, R., Moyroud, E., Rudall, P.J., Prychid, C.J., Conejero, M., Glover, B.J., and Vignolini, S. (2021). Using structural colour to track length scale of cell-wall layers in developing Pollia japonica fruits. New Phytol. *230*, 2327–2336.

10. Whitney, H.M., Kolle, M., Andrew, P., Chittka, L., Steiner, U., and Glover, B.J. (2009). Floral Iridescence, Produced by Diffractive Optics, Acts As a Cue for Animal Pollinators. Science *323*, 130–133.

11. Moyroud, E., Wenzel, T., Middleton, R., Rudall, P.J., Banks, H., Reed, A., Mellers, G., Killoran, P., Westwood, M.M., Steiner, U., et al. (2017). Disorder in convergent floral nanostructures enhances signalling to bees. Nature *550*, 469–474.

12. Vignolini, S., Moyroud, E., Hingant, T., Banks, H., Rudall, P.J., Steiner, U., and Glover, B.J. (2015). The flower of Hibiscus trionum is both visibly and measurably iridescent. New Phytol. *205*, 97–101.

13. Antoniou Kourounioti, R.L., Band, L.R., Fozard, J.A., Hampstead, A., Lovrics, A., Moyroud, E., Vignolini, S., King, J.R., Jensen, O.E., and Glover, B.J. (2013). Buckling as an origin of ordered cuticular patterns in flower petals. J. R. Soc. Interface *10*, 20120847.

14. Huang, X., Hai, Y., and Xie, W.-H. (2017). Anisotropic cell growth-regulated surface micropatterns in flower petals. Theor. Appl. Mech. Lett. *7*, 169–174.

15. Airoldi, C.A., Lugo, C.A., Wightman, R., Glover, B.J., and Robinson, S. (2021). Mechanical buckling can pattern the light-diffracting cuticle of Hibiscus trionum. Cell Rep. *36*, 109715.

16. Takahashi, K., Shimada, T., Kondo, M., Tamai, A., Mori, M., Nishimura, M., and Hara-Nishimura, I. (2010). Ectopic Expression of an Esterase, Which is a Candidate for the Unidentified Plant Cutinase, Causes Cuticular Defects in Arabidopsis thaliana. Plant Cell Physiol. *51*, 123–131.

17. Broun, P., Poindexter, P., Osborne, E., Jiang, C.-Z., and Riechmann, J.L. (2004). WIN1, a transcriptional activator of epidermal wax accumulation in Arabidopsis. Proc. Natl. Acad. Sci. *101*, 4706–4711.

18. Aharoni, A., Dixit, S., Jetter, R., Thoenes, E., van Arkel, G., and Pereira, A. (2004). The SHINE Clade of AP2 Domain Transcription Factors Activates Wax Biosynthesis, Alters Cuticle Properties, and Confers Drought Tolerance when Overexpressed in Arabidopsis. Plant Cell *16*, 2463–2480.

19. Kannangara, R., Branigan, C., Liu, Y., Penfield, T., Rao, V., Mouille, G., Höfte, H., Pauly, M., Riechmann, J.L., and Broun, P. (2007). The Transcription Factor WIN1/SHN1 Regulates Cutin Biosynthesis in Arabidopsis thaliana. Plant Cell *19*, 1278–1294.

20. Triezenberg, S.J., Kingsbury, R.C., and McKnight, S.L. (1988). Functional dissection of VP16, the trans-activator of herpes simplex virus immediate early gene expression. Genes Dev. *2*, 718–729.

21. Hiratsu, K., Ohta, M., Matsui, K., and Ohme-Takagi, M. (2002). The SUPERMAN protein is an active repressor whose carboxy-terminal repression domain is required for the development of normal flowers. FEBS Lett. *514*, 351–354.

22. Oshima, Y., Shikata, M., Koyama, T., Ohtsubo, N., Mitsuda, N., and Ohme-Takagi, M. (2013). MIXTA-Like Transcription Factors and WAX INDUCER1/SHINE1 Coordinately Regulate Cuticle Development in Arabidopsis and Torenia fournieri. Plant Cell *25*, 1609–1624.

23. Shi, J.X., Adato, A., Alkan, N., He, Y., Lashbrooke, J., Matas, A.J., Meir, S., Malitsky, S., Isaacson, T., Prusky, D., et al. (2013). The tomato SlSHINE3 transcription factor regulates fruit cuticle formation and epidermal patterning. New Phytol. *197*, 468–480.

24. Brockington, S.F., Alvarez-Fernandez, R., Landis, J.B., Alcorn, K., Walker, R.H., Thomas, M.M., Hileman, L.C., and Glover, B.J. (2013). Evolutionary Analysis of the MIXTA Gene Family Highlights Potential Targets for the Study of Cellular Differentiation. Mol. Biol. Evol. *30*, 526–540.

25. Go, Y.S., Kim, H., Kim, H.J., and Suh, M.C. (2014). Arabidopsis Cuticular Wax Biosynthesis Is Negatively Regulated by the DEWAX Gene Encoding an AP2/ERF-Type Transcription Factor. Plant Cell *26*, 1666–1680.

26. Fich, E.A., Segerson, N.A., and Rose, J.K.C. (2016). The Plant Polyester Cutin: Biosynthesis, Structure, and Biological Roles. Annu. Rev. Plant Biol. *67*, 207–233.

27. Girard, A.-L., Mounet, F., Lemaire-Chamley, M., Gaillard, C., Elmorjani, K., Vivancos, J., Runavot, J.-L., Quemener, B., Petit, J., Germain, V., et al. (2012). Tomato GDSL1 Is Required for Cutin Deposition in the Fruit Cuticle. Plant Cell *24*, 3119–3134.

28. Yeats, T.H., Martin, L.B.B., Viart, H.M.-F., Isaacson, T., He, Y., Zhao, L., Matas, A.J., Buda, G.J., Domozych, D.S., Clausen, M.H., et al. (2012). The identification of cutin synthase: formation of the plant polyester cutin. Nat. Chem. Biol. *8*, 609–611.

29. Yeats, T.H., Huang, W., Chatterjee, S., Viart, H.M.-F., Clausen, M.H., Stark, R.E., and Rose, J.K.C. (2014). Tomato Cutin Deficient 1 (CD1) and putative orthologs comprise an ancient family of cutin synthase-like (CUS) proteins that are conserved among land plants. Plant J. *77*, 667–675.

30. Hong, L., Brown, J., Segerson, N.A., Rose, J.K.C., and Roeder, A.H.K. (2017). CUTIN SYNTHASE 2 Maintains Progressively Developing Cuticular Ridges in Arabidopsis Sepals. Mol. Plant *10*, 560–574.

31. Huang, R. (2005). Kinetic wrinkling of an elastic film on a viscoelastic substrate. J. Mech. Phys. Solids *53*, 63–89.

32. Li, B., Cao, Y.-P., Feng, X.-Q., and Gao, H. (2012). Mechanics of morphological instabilities and surface wrinkling in soft materials: a review. Soft Matter *8*, 5728–5745.

33. Chen, C., Airoldi, C.A., Lugo, C.A., Bay, R.K., Glover, B.J., and Crosby, A.J. (2021). Flower Inspiration: Broad-Angle Structural Color through Tunable Hierarchical Wrinkles in Thin Film Multilayers. Adv. Funct. Mater. *31*, 2006256.

34. Giorio, C., Moyroud, E., Glover, B.J., Skelton, P.C., and Kalberer, M. (2015). Direct Surface Analysis Coupled to High-Resolution Mass Spectrometry Reveals Heterogeneous Composition of the Cuticle of Hibiscus trionum Petals. Anal. Chem. *87*, 9900–9907.

35. Li-Beisson, Y., Pollard, M., Sauveplane, V., Pinot, F., Ohlrogge, J., and Beisson, F. (2009). Nanoridges that characterize the surface morphology of flowers require the synthesis of cutin polyester. Proc. Natl. Acad. Sci. *106*, 22008–22013.

36. Panikashvili, D., Shi, J.X., Schreiber, L., and Aharoni, A. (2009). The Arabidopsis DCR Encoding a Soluble BAHD Acyltransferase Is Required for Cutin Polyester Formation and Seed Hydration Properties. Plant Physiol. *151*, 1773–1789.

37. Mazurek, S., Garroum, I., Daraspe, J., De Bellis, D., Olsson, V., Mucciolo, A., Butenko, M.A., Humbel, B.M., and Nawrath, C. (2017). Connecting the Molecular Structure of Cutin to Ultrastructure and Physical Properties of the Cuticle in Petals of Arabidopsis. Plant Physiol. *173*, 1146–1163.

38. Domínguez, E., España, L., López-Casado, G., Cuartero, J., and Heredia, A. (2009). Biomechanics of isolated tomato (Solanum lycopersicum) fruit cuticles during ripening: the role of flavonoids. Funct. Plant Biol. *36*, 613–620.

39. Bargel, H., Koch, K., Cerman, Z., and Neinhuis, C. (2006). Evans Review No. 3: Structure–function relationships of the plant cuticle and cuticular waxes — a smart material? Funct. Plant Biol. *33*, 893–910.

40. Tsubaki, S., Sugimura, K., Teramoto, Y., Yonemori, K., and Azuma, J. (2013). Cuticular Membrane of Fuyu Persimmon Fruit Is Strengthened by Triterpenoid Nano-Fillers. PLOS ONE *8*, e75275.

41. España, L., Heredia-Guerrero, J.A., Segado, P., Benítez, J.J., Heredia, A., and Domínguez, E. (2014). Biomechanical properties of the tomato (Solanum lycopersicum) fruit cuticle during development are modulated by changes in the relative amounts of its components. New Phytol. *202*, 790–802.

42. España, L., Heredia-Guerrero, J.A., Reina-Pinto, J.J., Fernández-Muñoz, R., Heredia, A., and Domínguez, E. (2014). Transient Silencing of CHALCONE SYNTHASE during Fruit Ripening Modifies Tomato Epidermal Cells and Cuticle Properties. Plant Physiol. *166*, 1371–1386.

43. Hunt, L., Amsbury, S., Baillie, A., Movahedi, M., Mitchell, A., Afsharinafar, M., Swarup, K., Denyer, T., Hobbs, J.K., Swarup, R., et al. (2017). Formation of the Stomatal Outer Cuticular Ledge Requires a Guard Cell Wall Proline-Rich Protein. Plant Physiol. *174*, 689–699.

44. Fernández, V., Guzmán-Delgado, P., Graça, J., Santos, S., and Gil, L. (2016). Cuticle Structure in Relation to Chemical Composition: Re-assessing the Prevailing Model. Front. Plant Sci. *7*.

45. van der Kooi, C.J., Wilts, B.D., Leertouwer, H.L., Staal, M., Elzenga, J.T.M., and Stavenga, D.G. (2014). Iridescent flowers? Contribution of surface structures to optical signaling. New Phytol. *203*, 667–673.

46. Murray, B.G., Craven, L.A., and De Lange, P.J. (2008). New observations on chromosome number variation in Hibiscus trionum s.l. (Malvaceae) and their implications for systematics and conservation. N. Z. J. Bot. *46*, 315–319.

47. Ren, M., Chen, Q., Li, L., Zhang, R., and Guo, S. (2005). Successive chromosome walking by compatible ends ligation inverse PCR. Mol. Biotechnol. *30*, 95–101.

48. Gibson, D.G., Young, L., Chuang, R.-Y., Venter, J.C., Hutchison, C.A., and Smith, H.O. (2009). Enzymatic assembly of DNA molecules up to several hundred kilobases. Nat. Methods *6*, 343–345.

49. Ganger, M.T., Dietz, G.D., and Ewing, S.J. (2017). A common base method for analysis of qPCR data and the application of simple blocking in qPCR experiments. BMC Bioinformatics *18*, 534.

50. Zielinski, A.T., Kourtchev, I., Bortolini, C., Fuller, S.J., Giorio, C., Popoola, O.A.M., Bogialli, S., Tapparo, A., Jones, R.L., and Kalberer, M. (2018). A new processing scheme for ultra-high resolution direct infusion mass spectrometry data. Atmos. Environ. *178*, 129–139.

51. Dray, S., and Dufour, A.-B. (2007). The ade4 Package: Implementing the Duality Diagram for Ecologists. J. Stat. Softw. *22*, 1–20.

52. R Core Team (2017). R: A language and environment for statistical computing. R Found. Stat. Comput. Vienna Austria. https://www.r-project.org/.

53. Altschul, S.F., Madden, T.L., Schäffer, A.A., Zhang, J., Zhang, Z., Miller, W., and Lipman, D.J. (1997). Gapped BLAST and PSI-BLAST: a new generation of protein database search programs. Nucleic Acids Res. *25*, 3389–3402.

54. Katoh, K., Misawa, K., Kuma, K., and Miyata, T. (2002). MAFFT: a novel method for rapid multiple sequence alignment based on fast Fourier transform. Nucleic Acids Res. *30*, 3059–3066.

55. Brown, J.W., Walker, J.F., and Smith, S.A. (2017). Phyx: phylogenetic tools for unix. Bioinformatics *33*, 1886–1888.

56. Kalyaanamoorthy, S., Minh, B.Q., Wong, T.K.F., von Haeseler, A., and Jermiin, L.S. (2017). ModelFinder: fast model selection for accurate phylogenetic estimates. Nat. Methods *14*, 587–589.

57. Nguyen, L.-T., Schmidt, H.A., von Haeseler, A., and Minh, B.Q. (2015). IQ-TREE: A Fast and Effective Stochastic Algorithm for Estimating Maximum-Likelihood Phylogenies. Mol. Biol. Evol. *32*, 268–274.

58. Minh, B.Q., Nguyen, M.A.T., and von Haeseler, A. (2013). Ultrafast Approximation for Phylogenetic Bootstrap. Mol. Biol. Evol. *30*, 1188–1195.

59. Robinson, S., Huflejt, M., Barbier de Reuille, P., Braybrook, S.A., Schorderet, M., Reinhardt, D., and Kuhlemeier, C. (2017). An Automated Confocal Micro-Extensometer Enables in Vivo Quantification of Mechanical Properties with Cellular Resolution. Plant Cell *29*, 2959–2973.

60. Abramoff, M.D., Magalhães, P.J., and Ram, S.J. (2004). Image processing with ImageJ. Biophotonics Int. *11*, 36–42.

Key resources table

REAGENT or RESOURCE	SOURCE	IDENTIFIER
Bacterial and virus strains		
Escherichia coli DH5α competent cells	ThermoFisher	Cat# 18265017
ElectroMAX™ *Agrobacterium tumefaciens* LBA4404	ThermoFisher	Cat# 18313015
Chemicals, peptides, and recombinant proteins		
Phusion® High-Fidelity DNA Polymerase	New England Biolabs	M0530L
EcoRV	New England Biolabs	R0195S
EcoRI	New England Biolabs	R0101S
T5 Exonuclease (for Gibson Assembly)	New England Biolabs	M0663S
Taq DNA ligase (for Gibson Assembly)	New England Biolabs	M0208S
Plant Agar	Sigma-Aldrich	A7921
Kanamycin	Sigma-Aldrich	BP861
Streptomycin	Sigma-Aldrich	S9137
MS salts with vitamins	Duchefa	M0222
Acetosyringone	Sigma-Aldrich	D134406
L-cysteine	Sigma-Aldrich	168149
L-Ascorbic acid	Sigma-Aldrich	A4544
Thidiazuron (TDZ)	Sigma-Aldrich	P6186
6-Benzylaminopurine (BA)	Sigma-Aldrich	B3408
Cefotaxime	Sigma-Aldrich	C7039
Glutaraldhehyde	Sigma-Aldrich	G7651
Sudan Red 7B	Sigma-Aldrich	201618
Lanolin	Sigma-Aldrich	L7387
3-indoleacetic acid (IAA)	Sigma-Aldrich	I3750
Gibberelic acid, 98%	Fischer scientific	15402377
NPA	Sigma-Aldrich	PS343
Taxol	Sigma-Aldrich	PHL89806
Oryzalin	Sigma-Aldrich	36182
Formic acid	Sigma-Aldrich	695076
Acetonitrile	Sigma-Aldrich	34851
Chloroform	Sigma-Aldrich	366927
Critical commercial assays		
Spectrum™ Plant Total RNA kit	Sigma-Aldrich	STRN50
SuperScript™ III First-strand synthesis system	Invitrogen	18080051
SuperScript™ II Reverse Transcriptase	Invitrogen	18064071
Luna® Universal qPCR Master Mix	New England Biolabs	M3003L
Deposited data		
HtSHINE1 sequence	GenBank	MW801439
HtSHINE2 sequence	GenBank	MW801440
HtSHINE3 sequence	GenBank	MW801441
HtMIXTA-like1 sequence	GenBank	MW801437
HtCUS1 sequence	GenBank	MW801438
Experimental models: Organisms/strains		
Hibiscus trionum, L.	Chiltern seeds (UK)	Cat No. 688K
Hibiscus sabdariffa	Chiltern seeds (UK)	Cat No. 688A
Hibiscus panduriformis	Sunshine seeds (Germany)	N/A
Hibiscus cannabinus	Jungle seeds (UK)	JS628

Hibiscus trionum (commercial)	[45]	N/A
Hibiscus richardsonii (Mayor Island (Tuhua), New Zealand)	[46]	Voucher AK251841
Hibiscus trionum New Zealand 'naturalised race' (Bream Head, North island, New Zealand)	[46]	Voucher AK253689
Hibiscus trionum (Botswana)	Millennium Seed Bank	Acc. Nb 91154
Hibiscus trionum, L: 2xp35S::AtCDEF1	This study	N/A
Hibiscus trionum, L: 2xp35S::AtDEWAX	This study	N/A
Hibiscus trionum, L: 2xp35S::HtSHN3-VP16	This study	N/A
Hibiscus trionum, L: 2xp35S::HtSHN3-SRDX	This study	N/A
Hibiscus trionum, L: 2xp35S::HtMIXTA-like1	This study	N/A
Hibiscus trionum, L: 2xp35S::HtCUS1	This study	N/A
Hibiscus trionum, L: pAtUBQ10::HtSHN3	This study	N/A
Oligonucleotides		
See Data S3 for Oligonucleotides		
Recombinant DNA		
Modified pGreen II 0229 with *2xp35S*	This study	N/A
Modified pGreen II 0229 with *2xp35S* and *pUBQ10::eYFPmyr*	This study	pEM110
AtCDEF1 in pBluescript KS(-)	This study	pEM111
2xp35S::AtCDEF1 in pEM110	This study	pEM112
HtSHN3 in pBluescript KS(-)	This study	pEM75
pAtUBQ10::HtSHN3 in pGreen II 0229	This study	pEM76
2xp35S::HtSHN3-VP16 in pEM110	This study	pEM114
2xp35S::HtSHN3-SRDX in pEM110	This study	pEM115
HtMIXTA-like1 in pBluescript KS(-)	This study	pEM85
2xp35S::HtMIXTA-like1 in pEM110	This study	pEM109
HtCUS1 in pBluescript KS(-)	This study	pEM99
2xp35S::HtCUS1 in pGreen II 0229	This study	pEM100
AtDEWAX pBluescript KS(-)	This study	pEM97
2xp35S::AtDEWAX in pGreen II 0229	This study	pEM98
Software and algorithms		
ImageJ	[60]	https://imagej.nih.gov/ij/
ACME controller software ACMErobotX	[59]	https://github.com/ACME-Robinson/InstallPackage
BLASTP	[53]	N/A
MAFFT v7.271	[54]	N/A
phyx v.0.999	[55]	N/A
IQtree v1.6.3	[57]	N/A
R	R Core Team, [52]	N/A
ade4 package	[51]	N/A
Xcalibur 2.1	Thermo Scientific, [34] and [50]	N/A
Mathematica 10	Wolfram research Inc., UK and [34]	N/A
Other		
Keyence VHX-5000 microscope with a VH-Z20, a VH-Z100 and a VH-Z500 lenses	Keyence	N/A
Automated Confocal Micro-Extensometer (ACME)	[59]	N/A

Tough tags	DiversifiedBiotech	TTSW-1000
Hitachi S-4700 Cryo-SEM	Hitachi	N/A
Zeiss EVO HD 15 equipped with the Quorum PP3010T cryo apparatus	Zeiss	N/A
Leica stereomicroscope M205FA	Leica	N/A
PlantEnsembl	http://plants.ensembl.org	N/A

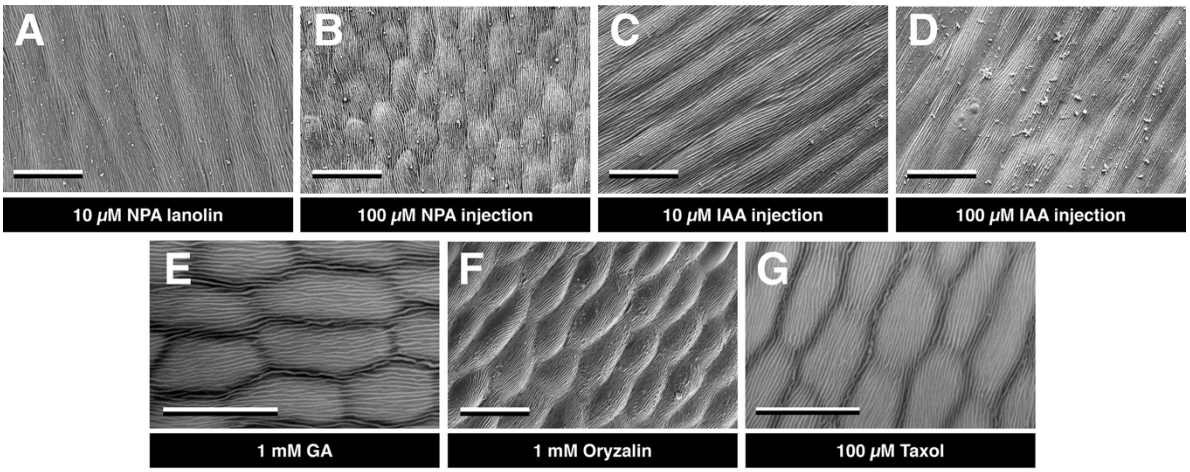

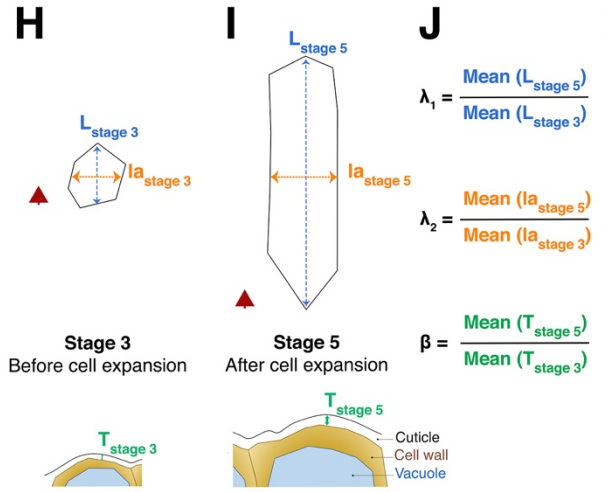

K

Treatment	Average Cell Length (μm) ± s.e	Average Cell Width (μm) ± s.e
Lanolin only	74.7 (± 2.1)	22.8 (± 0.6)
10 μM IAA lanolin	74.2 (± 1.8)	25.5 (± 1.1)
50 μM IAA lanolin	70.4 (± 2.1)	23.3 (± 0.8)
100 μM IAA lanolin	64.9 (± 2.4)	20.3 (± 0.7)
50 μM IAA injection	75.4 (± 2.8)	23.3 (± 0.7)
10 μM IAA injection	78.9 (± 1.9)	26.4 (± 0.8)
100 μM IAA injection	66.9 (± 2.6)	20.8 (± 0.6)
10 μM NPA lanolin	76.8 (± 2.1)	23.2 (± 0.7)
30 μM NPA lanolin	74.4 (± 2.5)	25.9 (± 0.8)
50 μM NPA lanolin	67.5 (± 2.3)	23.7 (± 1.1)
30 μM NPA injection	64.9 (± 2.1)	24.5 (± 0.9)
10 μM NPA injection	67.4 (± 2.5)	21.5 (± 0.7)
50 μM NPA injection	59.9 (± 2.4)	22.9 (± 0.7)
100 μM NPA injection	34.4 (± 1.2)	17.2 (± 0.6)
1 mM GA lanolin	54.2 (± 2.3)	20.5 (± 0.9)
100 μM Oryzalin lanolin	68.4 (± 1.9)	21.1 (± 0.7)
1 mM Oryzalin lanolin	44.2 (± 1.6)	18.5 (± 0.6)
50 μM taxol lanolin	56.1 (± 2.0)	23.3 (± 0.6)
100 μM taxol lanolin	53.3 (± 2.9)	20.9 (± 0.7)

Figure S1. Application of drugs or hormones on developing buds of *H. trionum* modified cell dimensions in the proximal region of the petal but did not prevent striation formation in the cuticle, Related to Figure 2A, D-F and Figure 4J, K. Scanning electron microscopy images representative of the proximal region of Stage 5 petals (open flower) after application of 10 μM NPA in lanolin at the base of a Stage 3 bud (**A**), 100 μM NPA solution injected between sepals and petals of a stage 3 bud (**B**), 10 μM (**C**) or 100 μM (**D**) NPA solution injected between sepals and petals of a stage 3 bud, or 1 mM GA (**E**), 1 mM Oryzalin (**F**) or 100 μM Taxol (**G**) in lanolin at the base of Stage 3 buds. Treatments modified cell dimensions (Table S1), but all conditions led to the production of a striated cuticle. Scale bars are all 50 μm. **(H-J)** Measurement of cell dimensions and cuticle thickness before and after cell expansion. (**H**) Cell length ($L_{stage\ 3}$), width ($la_{stage\ 3}$) and cuticle thickness ($T_{stage\ 3}$) measured on cells from stage 3 petal epidermis. (**I**) Cell length ($L_{stage\ 5}$), width ($la_{stage\ 5}$) and cuticle thickness ($T_{stage\ 5}$) measured on cells from stage 5 petal epidermis. (**J**) Calculation of expansion λ_1 and λ_2 and β factors as described in the Methods section. (**K**) Cell dimensions in open *H. trionum* flowers (Stage 5) after application of drugs or hormone treatments.

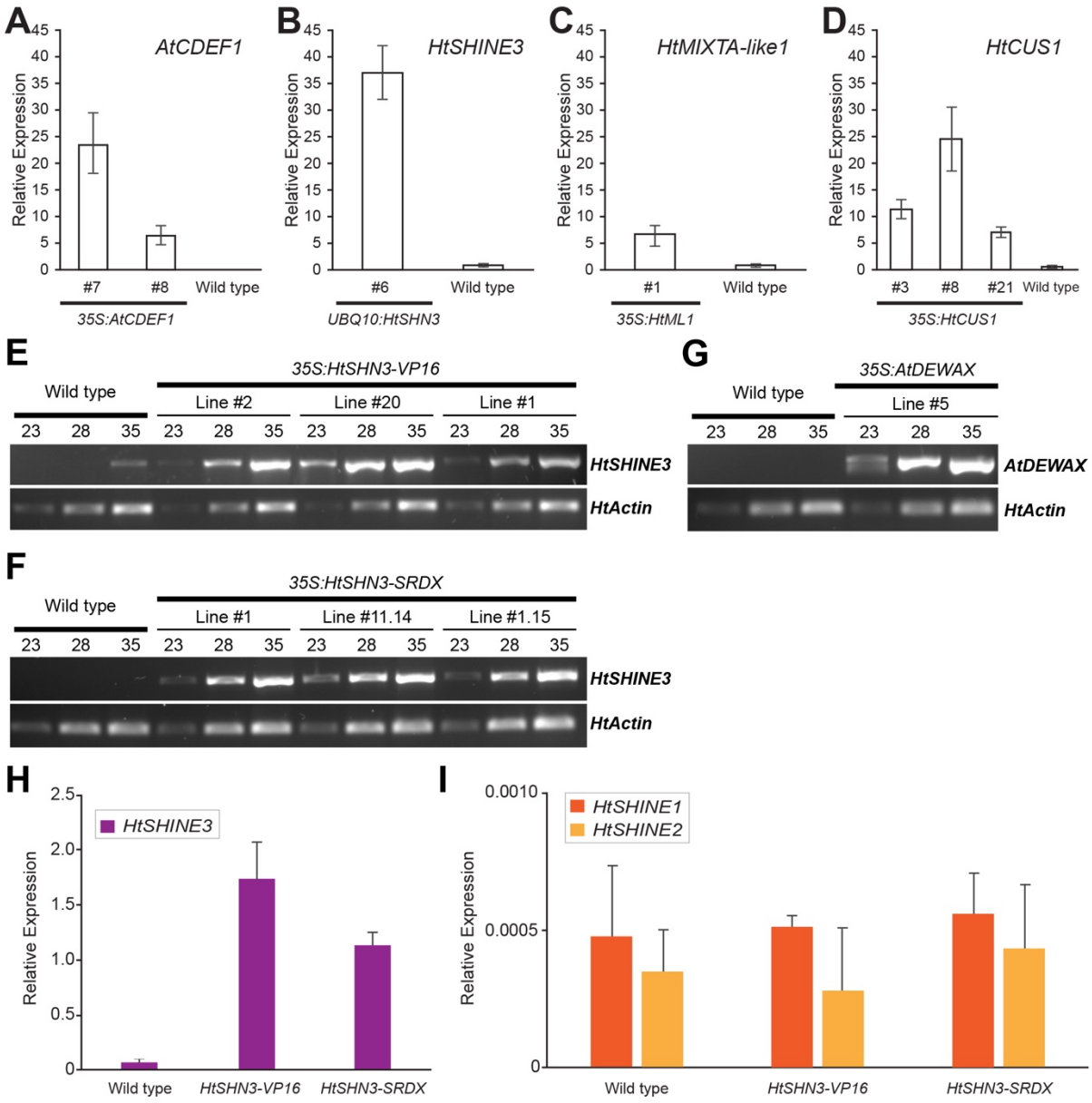

Figure S2. Transgene and gene expression in *Hibiscus trionum* transgenic lines, Related to Figures 3, Figure 4 and Figure 5. Relative expression levels of *AtCDEF1* (**A**), *HtSHINE3* (**B**), *HTMIXTA-Like1* (**C**) and *HtCUS1* (**D**) normalised to *HtActin* in various transgenic lines and *H. trionum* wild type. The mean of 3 biological replicates is indicated for each line. Error bars represent 1 Standard Deviation. No expression of *AtCDEF1* was detected in wild type plants. (**E-G**) Transgene expression in *35S:HtSHINE3-VP16, 35S:HtSHINE3-SRDX* and *35S:AtDEWAX Hibiscus trionum* transgenic lines. Reverse transcription-polymerase chain reaction (RT-PCR) profiles of *HtSHN3-VP16* (**E**), *HtSHN3-SRDX* (**F**) and *AtDEWAX* (**G**) in leaves of wild type (control) and corresponding transgenic lines. *HtActin* was used as a control. PCR cycles are given above each lane. (**H-I**) Expression levels of *HtSHINE* genes in

the proximal region of stage 3 petals from wild type individuals and transgenic plants overexpressing *HtSHINE3-VP16* or *HtSHINE3-SRDX.* Relative expression levels of *HtSHN3*, *HtSHN1* and *HtSHN2* normalised to *HtActin* in *H. trionum* wild type, *35S:HtSHN3-VP16* (T3 generation) and *35S:HtSHN3-SRDX* (T3 generation). The mean of 4 biological replicates is indicated for each line. Error bars represent 1 Standard Deviation.

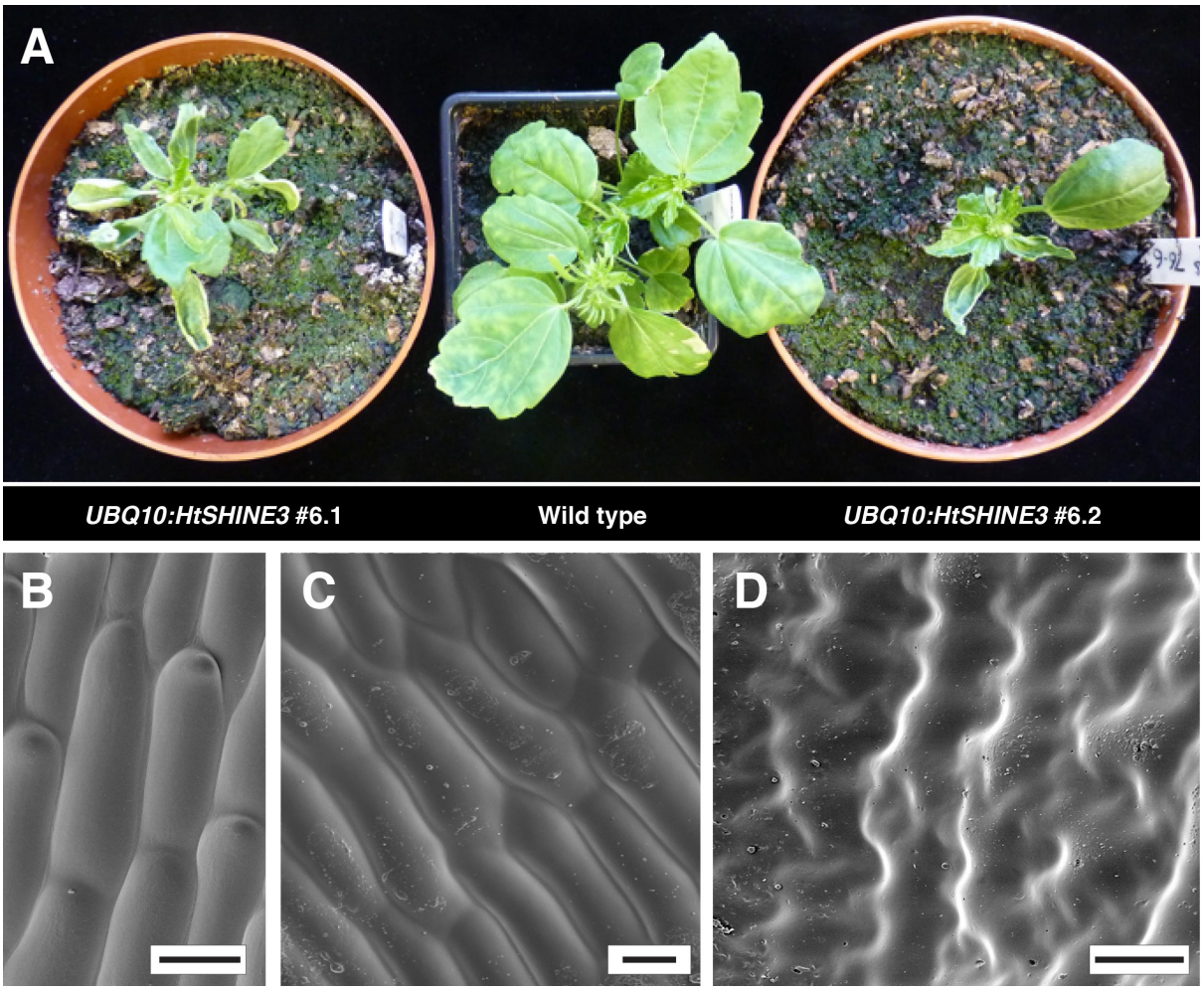

Figure S3. Vegetative phenotype of *UBQ10:HtSHINE3* transgenic *H. trionum* lines, Related to Figure 3. (**A**) Constitutive expression of *HtSHINE3* induces some growth defects in *H. trionum*. The plants are smaller and produce narrower leaves with frequently curled margins. Those leaves also appear rough and thicker than wild type leaves. SEM imaging of the boundary region (**B**) on the adaxial (upper) petal epidermis, or of the proximal (**C**) and distal (**D**) regions on the abaxial (lower) epidermis of flowers from wild type *H. trionum* showing that the abaxial epidermis and the adaxial boundary region are completely smooth in wild type. Scale bars are all 20μm.

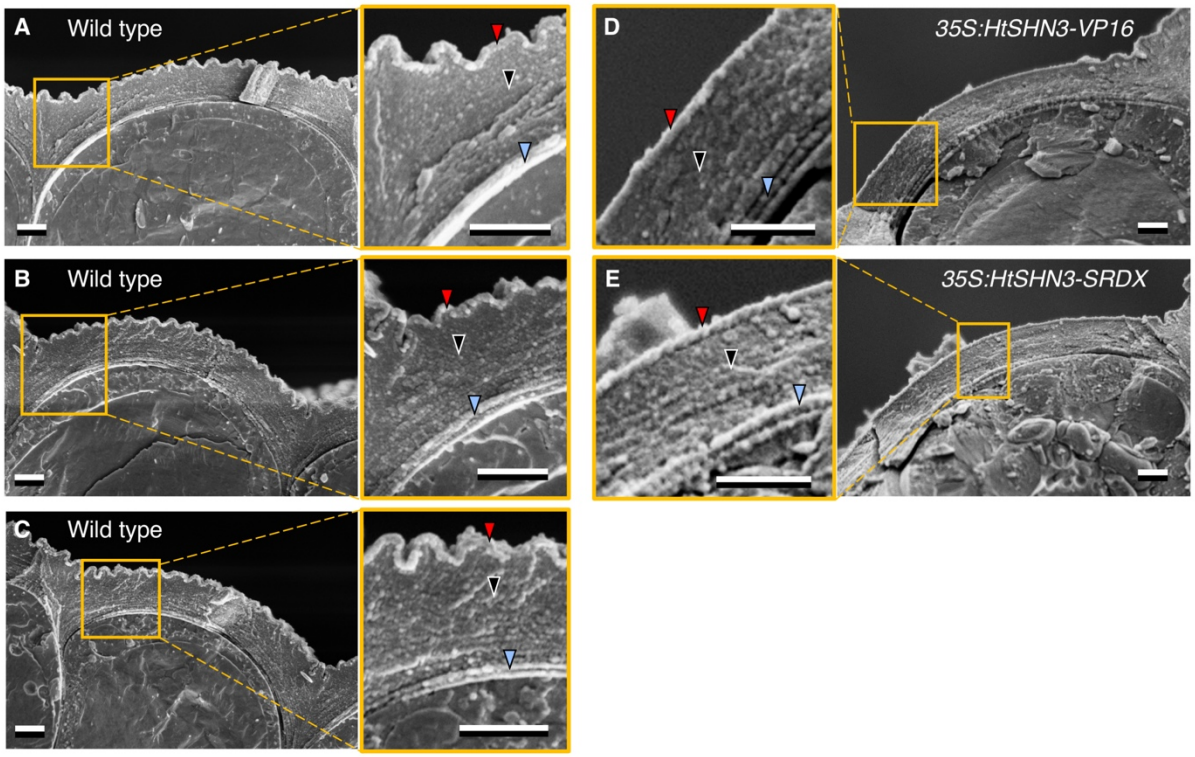

Figure S4. CryoSEM fractures of the proximal petal region (adaxial epidermis) of wild type (A-C), *35S:HtSHN3-VP16* (D) and *35S:HtSHN3-SRDX* (E) *H. trionum* lines, Related to Figure 4. (**A**) Red and black arrows indicate the cuticle proper and cuticular layer, respectively, and blue arrows indicate the cell wall as defined in [S1]. Scale bars = 2 μm.

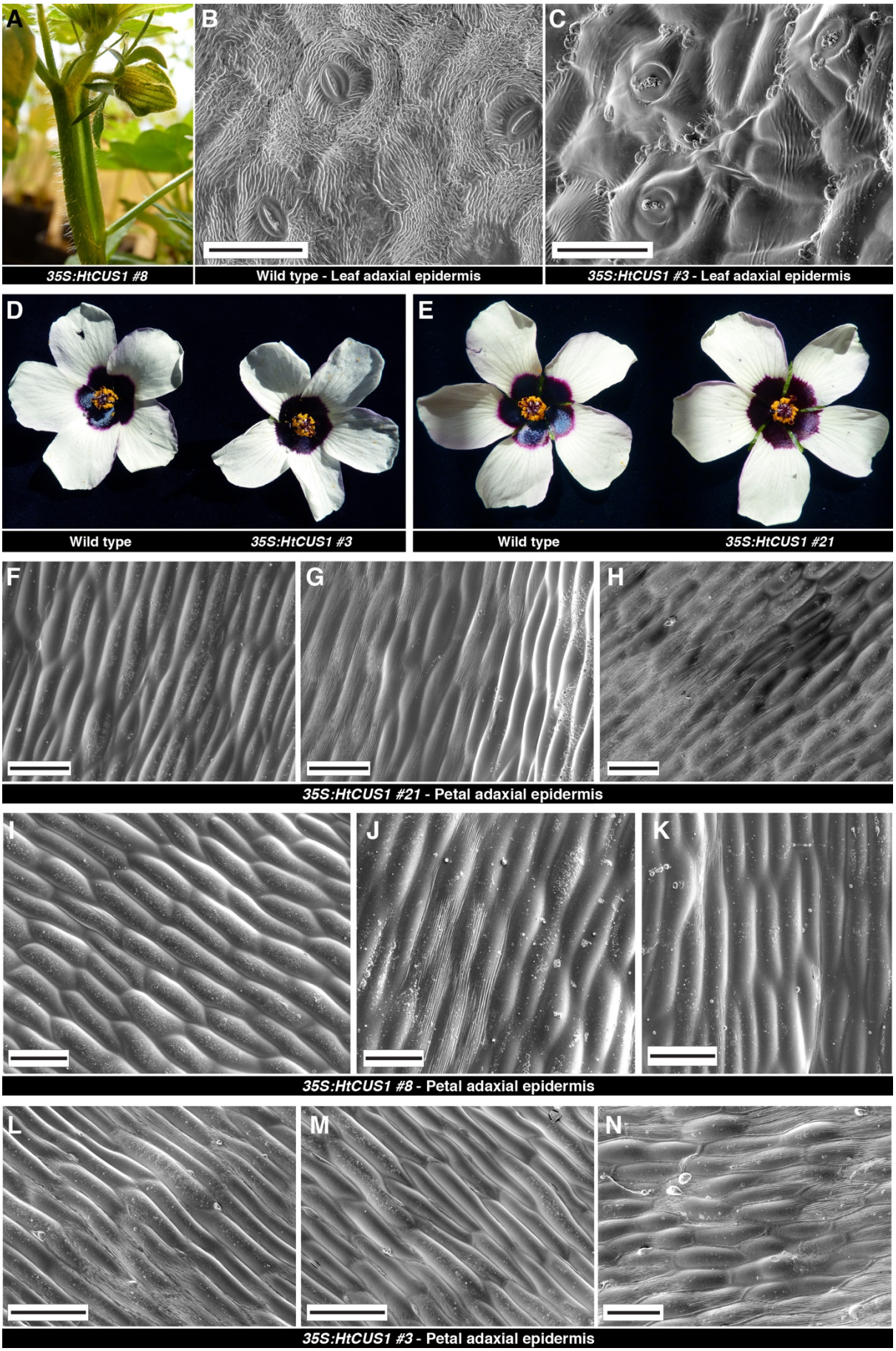
A
B
C
35S:HtCUS1 #8
Wild type - Leaf adaxial epidermis
35S:HtCUS1 #3 - Leaf adaxial epidermis
D
E
Wild type
35S:HtCUS1 #3
Wild type
35S:HtCUS1 #21
F
G
H
35S:HtCUS1 #21 - Petal adaxial epidermis
I
J
K
35S:HtCUS1 #8 - Petal adaxial epidermis
L
M
N
35S:HtCUS1 #3 - Petal adaxial epidermis

Figure S5. Vegetative and floral phenotype of *35S:HtCUS1* transgenic *H. trionum* lines, Related to Figure 5. (**A**) Abnormal fusion between peduncle and stem in *35S:HtCUS1* (line #8). (**B**) SEM image of the adaxial surface of *H. trionum* leaves. All cells, except stomatal guard cells, are covered with prominent cuticular striations. (**C**) SEM image of the adaxial surface of a leaf from *35S:HtCUS1* (line #3) transgenic *H. trionum*. Cuticular striations are either absent or faint. (**D**) Flower of *35S:HtCUS1* (line #3) and (**E**) flower of *35S:HtCUS1* (line #21), note the absence of conspicuous blue sheen in the pigmented proximal region of the corolla compared to wild type flowers imaged side-by-side. (**F-N**) SEM images of the adaxial surface of the petal proximal region from three independent *35S:HtCUS1* transgenic *H. trionum* lines. Depending on the line and individual flower, the striations normally present in the equivalent region in wild type petal (see Figure 3I) are absent, patchy or faint. (F-H) *35S:HtCUS1*(line #21), (I-K) *35S:HtCUS1*(line #8) and (L-N) *35S:HtCUS1* (line #3). Scale bars B-C and F-M = 50 μm.

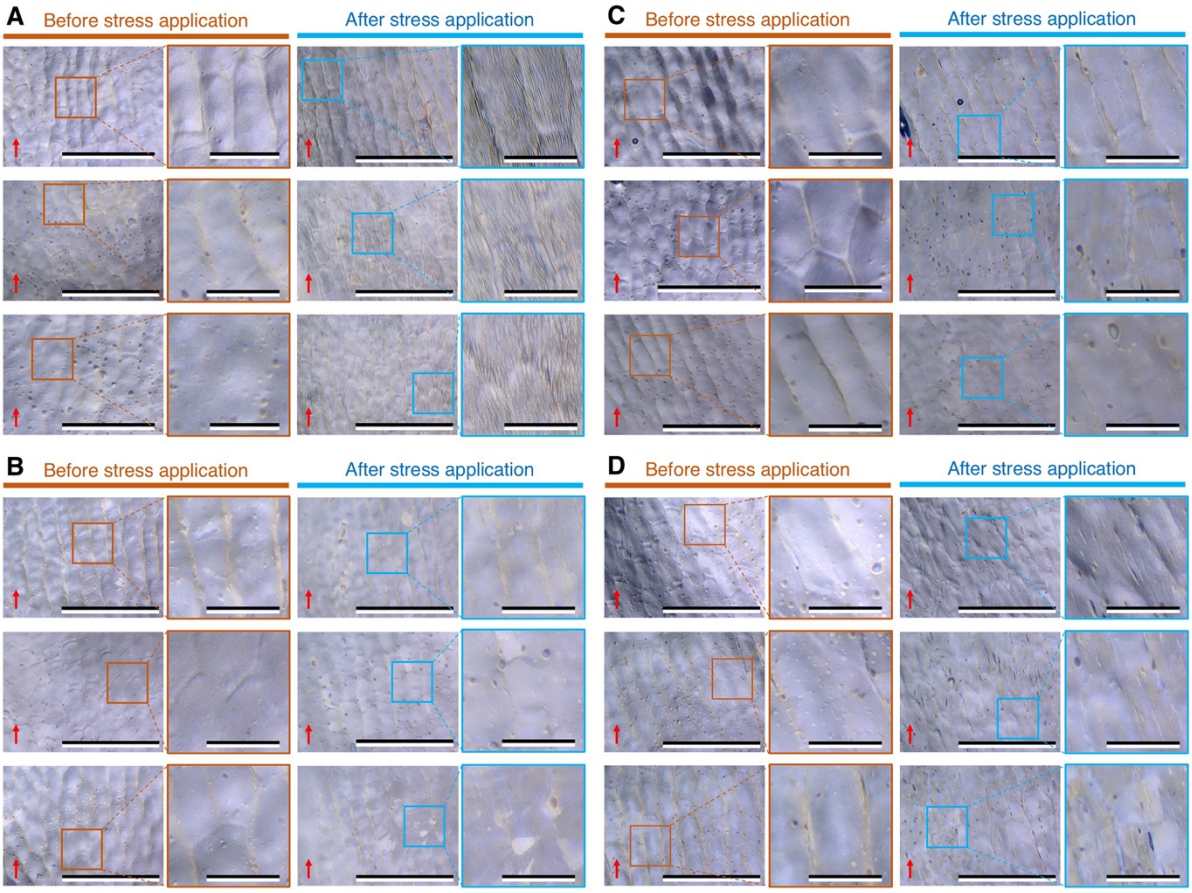

E

Genotype	Sample #	Developmental stage	Sample width (μm)	Force (mN)	Strain (%)
Wild type	1	Stage 3, 11-12 mm	731	64	25
	2	Stage 3, 11-12 mm	818	64	13
	3	Stage 3, 11-12 mm	796	64	11
35S:HtSHN3-VP16	1	Stage 3, 11-12 mm	654	64	31
	2	Stage 3, 11-12 mm	806	61	21
	3	Stage 3, 11-12 mm	722	61	14
35S:HtSHN3-EAR	1	Stage 3, 11-12 mm	821	64	19
	2	Stage 3, 11-12 mm	747	63	26
	3	Stage 3, 11-12 mm	771	64	12
35S:HtSHN3-VP16	1	Stage 4, 16-17 mm	901	65	20
	2	Stage 4, 16-17 mm	763	65	16
	3	Stage 4, 16-17 mm	724	65	27

Figure S6. Mechanical Perturbations, Related to Figure 4 and Figure 6. Adaxial petal tissue (proximal region) before (brown) and after (blue) longitudinal stress application. In each case, three experimental replicates using tissues from different plants are shown. For each replicate, a wide view of the sample surface and a closer view are provided next to each other. (**A**) *H. trionum* wild type, stage 3; (**B**) *35S:HtSHN3-SRDX*, stage 3; (**C**) *35S:HtSHN3-VP16*, stage 3 and (**D**) *35S:HtSHN3-VP16*, stage 4. Red arrows indicate the base-to-tip axis of the petal for orientation purposes. Scale bars in wide view images = 100 μm, Scale bars in closer view images = 25 μm. (**E**) Summary of the mechanical perturbations applied to petal primordia tissues from wild type (A) and transgenic (B-D) *H. trionum* flowers. The width of samples and force applied in each case are given.

Species/Line	Average Cell Length at Stage 3 (µm) ± s.e	Average Cell Length at Stage 5 (µm) ± s.e
H. trionum wild type	22.5 (± 1.1)	79.9 (± 4.3)
H. trionum commercial	15.5 (± 0.4)	75.7 (± 1.3)
H. trionum New Zealand	21.0 (± 1.2)	68.0 (± 2.3)
H. richardsonii	28.0 (± 0.9)	64.4 (± 1.8)
H. cannabinus	36.8 (± 1.3)	103.0 (± 3.9)
H. sabdariffa	24.2 (± 0.7)	68.5 (± 3.1)
H. panduriformis	24.9 (± 1.1)	105.2 (± 3.1)
H. trionum Botswana	34.1 (± 1.3)	95.4 (± 4.1)
35S:HtSHN3-SRDX	21.4 (± 0.9)	84.7 (± 3.4)
35S:HtSHN3-VP16	25.3 (± 1.6)	86.8 (± 3.7)
35S:HtMIXTA-like1	20.1 (± 0.8)	74.0 (± 2.7)

Species/Line	Average Cell Width at Stage 3 (µm) ± s.e	Average Cell Width at Stage 5 (µm) ± s.e
H. trionum wild type	13.9 (± 0.4)	25.0 (± 2.0)
H. trionum commercial	8.9 (± 0.4)	16.6 (± 0.3)
H. trionum New Zealand	13.0 (± 0.4)	21.5 (± 0.6)
H. richardsonii	17.0 (± 0.7)	24.2 (± 0.8)
H. cannabinus	26.0 (± 0.7)	37.7 (± 1.1)
H. sabdariffa	22.4 (± 0.6)	39.6 (± 1.2)
H. panduriformis	18.0 (± 0.6)	31.2 (± 0.8)
H. trionum Botswana	23.5 (± 0.6)	29.2 (± 1.1)
35S:HtSHN3- SRDX	16.7 (± 0.6)	21.2 (± 0.7)
35S:HtSHN3-VP16	16.8 (± 0.9)	19.1 (± 0.6)
35S:HtMIXTA-like1	14.6 (± 0.5)	20.7 (± 0.9)

Species/Line	Average Cuticle Thickness at Stage 3 (nm) ± s.e	Average Cuticle Thickness at Stage 5 (nm) ± s.e	β factor
H. trionum wild type	737 (± 11)	630 (± 10)	0.85
H. trionum commercial	634 (± 12)	567 (± 12)	0.89
H. trionum New Zealand	782 (± 32)	760 (± 19)	0.97
H. richardsonii	580 (± 22)	609 (± 18)	1.05
H. cannabinus	829 (± 24)	580 (± 20)	0.70
H. sabdariffa	749 (± 19)	816 (± 31)	1.09
H. panduriformis	402 (± 15)	894 (± 34)	2.23
H. trionum Botswana	878 (± 37)	812 (± 17)	0.92
35S:HtSHN3- SRDX	1061 (± 31)	1116 (± 59)	1.05
35S:HtSHN3-VP16	1060 (± 30)	726 (± 24)	0.68
35S:HtMIXTA-like1	779 (± 42)	821 (± 32)	1.05

Table S1. Average cell length, cell width and cuticle thickness (see Methods and Figure S1H-J) at Stage 3 (before cell expansion) and Stage 5 (after cell expansion) in different accessions and species from the Trionum and Phylloglandula sections of the *Hibiscus* phylogeny and in *H. trionum* transgenic lines, Related to Figure 2 and Figure 4.

A	Contribution to PC1 (%)	Cuticle type	% of striated samples with compound	% of smooth samples with compound
$C_{27}H_{28}O_{19}$	2.01	Smooth	25 (1/4)	90 (28/31)
$C_{12}H_{24}O_{12}$	1.96	Smooth	0 (0/4)	77 (24/31)
$C_{27}H_{28}O_{18}$	1.88	Smooth	25 (1/4)	94 (29/31)
$C_{16}H_{32}O_4$	1.73	Striated	100 (4/4)	19 (6/31)
$C_{26}H_{26}O_{17}$	1.72	Smooth	50 (2/4)	94 (29/31)
$C_{32}H_{56}O_4$	1.72	Striated	100 (4/4)	39 (12/31)
$C_{26}H_{26}O_{18}$	1.72	Smooth	25 (1/4)	94 (29/31)
$C_{51}H_{76}O_{12}$	1.61	Striated	100 (4/4)	23 (7/31)
$C_{18}H_{34}O_{17}$	1.58	Smooth	0 (0/4)	68 (21/31)
$C_{28}H_{50}O_4$	1.57	Striated	75 (3/4)	3 (1/31)
$C_{30}H_{54}O_4$	1.57	Striated	100 (4/4)	58 (18/31)
$C_{36}H_{66}O_4$	1.57	Striated	100 (4/4)	74 (23/31)
$C_{34}H_{60}O_4$	1.53	Striated	100 (4/4)	42 (13/31)
$C_{30}H_{54}O_3$	1.53	Striated	100 (4/4)	94 (29/31)
$C_{33}H_{42}O_{24}$	1.50	Smooth	0 (0/4)	65 (20/31)
$C_{30}H_{52}O_4$	1.49	Striated	100 (4/4)	29 (9/31)
$C_{28}H_{50}O_3$	1.46	Striated	50 (2/4)	16 (5/31)
$C_{36}H_{64}O_4$	1.43	Striated	100 (4/4)	39 (12/31)
$C_{32}H_{58}O_3$	1.41	Striated	100 (4/4)	84 (26/31)
$C_{34}H_{62}O_3$	1.40	Striated	75 (3/4)	10 (3/31)

B	Contribution to PC1 (%)	Cuticle type	% of striated samples with compound	% of smooth samples with compound
$C_{36}H_{66}O_4$	2.37	Striated	100 (12/12)	44 (11/25)
$C_{38}H_{70}O_4$	2.31	Striated	83 (10/12)	20 (5/25)
$C_{30}H_{54}O_4$	2.10	Striated	92 (11/12)	40 (10/25)
$C_{16}H_{32}O_4$	2.07	Striated	92 (11/12)	12 (3/25)
$C_{32}H_{56}O_4$	2.02	Striated	92 (11/12)	44 (11/25)
$C_{34}H_{60}O_4$	1.99	Striated	92 (11/12)	36 (9/25)
$C_{36}H_{64}O_4$	1.99	Striated	83 (10/12)	32 (8/25)
$C_{51}H_{76}O_{12}$	1.97	Striated	58 (7/12)	4 (1/25)
$C_{40}H_{72}O_9$	1.93	Striated	83 (10/12)	24 (6/25)
$C_{12}H_{24}O_{12}$	1.88	Smooth	58 (7/12)	84 (21/25)
$C_{53}H_{80}O_{12}$	1.86	Striated	42 (5/12)	4 (1/25)
$C_{38}H_{68}O_5$	1.85	Striated	42 (5/12)	0 (0/25)
$C_{47}H_{68}O_{12}$	1.84	Striated	58 (7/12)	32 (8/25)
$C_{27}H_{28}O_{19}$	1.78	Smooth	50 (6/12)	92 (23/25)
$C_{49}H_{72}O_{12}$	1.76	Striated	58 (7/12)	24 (6/25)
$C_{27}H_{28}O_{18}$	1.73	Smooth	25 (3/12)	92 (23/25)

Table S2. List of top compounds from (A) *H. trionum* wild type and transgenic lines contributing to PC1 in Figure 6A or from (B) *H. trionum* wild type and related Hibiscus species contributing to PC1 in Figure 6B, Related to Figure 2B-C and Figure 6.

Individual contribution to PC1 is given in the second column. Column 3 indicates whether the compound is typical of smooth or striated cuticle. Column 4 and 5 give the percentage of

striated (grey rows) and smooth (white rows) samples, respectively, for which the compound was detected (with samples for which compound was detected *vs*. total number of samples analysed in brackets). Compounds significantly associated with presence/absence of striations on the petal surface of both (A) transgenic *H. trionum* lines and (B) other Hibiscus species have been highlighted in turquoise (striated) and yellow (smooth), respectively.

Supplementary Reference

S1. Airoldi, C.A., Lugo, C.A., Wightman, R., Glover, B.J., and Robinson, S. (2021). Mechanical buckling can pattern the light-diffracting cuticle of Hibiscus trionum. Cell Rep. *36*, 109715. 10.1016/j.celrep.2021.109715.

S2. Pfeil, B.E., Crisp, M.D., Pfeil, B.E., and Crisp, M.D. (2005). What to do with Hibiscus? A proposed nomenclatural resolution for a large and well known genus of Malvaceae and comments on paraphyly. Aust. Syst. Bot. *18*, 49–60.

S3. Nakano, T., Suzuki, K., Fujimura, T., and Shinshi, H. (2006). Genome-Wide Analysis of the ERF Gene Family in Arabidopsis and Rice. Plant Physiol. *140*, 411–432.